

Behind-the-Meter Storage

Anthony Burrell

National Renewable Energy Laboratory
15013 Denver West Parkway
Golden, CO 80401
Phone: (303) 384-6666
E-mail: anthony.burrell@nrel.gov

Samuel Gillard, DOE-EERE-VTO

Technology Manager, Battery R&D
Phone: (202) 287-5849
E-mail: samuel.gillard@ee.doe.gov

Start Date: 1 October 2018

End Date: 30 September 2022

Project Funding (FY18): \$2,200K

DOE share: \$2,200K

Non-DOE share: \$0

Table of Contents

	Page
Overview	1
BTMS Analysis	4
Electrical and Thermal Design Behind-the-Meter System	11
BTMS Testing Section	18
Physics-Based Machine Learning for Behind-the-Meter Storage	25
Appendix: Description of BTMS Buildings Work	31

Project Introduction

This initiative, referred to as Behind-the-Meter Storage (BTMS), will focus on novel critical-materials-free battery technologies to facilitate the integration of electric vehicle (EV) charging, solar power generation technologies, and energy-efficient buildings while minimizing both costs and grid impacts. For extreme fast-charging at levels of 350 kW or higher, novel approaches are required to avoid significant negative cost and resiliency impacts. However, it is reasonable to assume that BTMS solutions would be applicable to other intermittent renewable energy generation sources or short-duration, high power-demand electric loads. BTMS research is targeted at developing innovative energy-storage technology specifically optimized for stationary applications below 10 MWh that will minimize the need for significant grid upgrades. Additionally, avoiding excessive high-power draws will eliminate excess demand charges that would be incurred during 350-kW fast-charging using current technologies. The key to achieving this is to leverage battery storage solutions that can discharge at high power but be recharged at standard lower power rates, acting as a power reservoir to bridge to the grid and other on-site energy generation technologies such as solar photovoltaics (PV), thereby minimizing costs and grid impacts. To be successful, new and innovative integration treatments must be developed for seamless interaction between stationary storage, PV generation, building systems, and the electric grid.

Key components of BTMS will address early-stage research into new energy-generation and building-integration concepts, critical-materials-free battery energy-storage chemistries, and energy-storage designs with a focus on new stationary energy-storage strategies that will balance performance and costs for expanded fast-charging networks while minimizing the need for grid improvements.

Objectives

A cohesive multidisciplinary research effort to create a cost-effective, critical-materials-free solution to BTMS by employing a whole-systems approach will be taken. The focus of this initiative is to develop innovative battery energy-storage technologies with abundant materials applicable to EVs and high-power charging systems. Solutions in the 1–10 MWh range will eliminate potential grid impacts of high-power EV charging systems as well as lower installation costs and costs to the consumer.

Although many lessons learned from EV battery development may be applied to the BTMS program, the requirements for BTMS systems are unique—carrying their own calendar-life, cycle-life, and cost challenges. For example, EV energy-storage systems need to meet very rigorous energy-density and volume requirements to meet consumer transportation needs. Despite that, current stationary storage systems use batteries designed for EVs due to high volumes driving down costs. This creates another market demand for EV batteries, further straining the EV battery supply chain and critical-material demand.

By considering BTMS electrochemical solutions optimized for these applications with less focus on energy density in mass and volume, the potential for novel battery solutions is very appealing. Furthermore, the balance-of-plant (BOP) for a BTMS battery system, or the cost of everything minus the battery cells, is thought to be upwards of 60% of the total energy-storage system cost. In contrast, the EV's BOP costs make up roughly 30% of the total battery cost. Therefore, BTMS will also need to focus on reducing BOP cost through system optimization to realize desired cost targets.

The design parameters are needed to optimize the BTMS system for performance, reliability, resilience, safety, and cost.

The objectives for the project are to:

- Produce BTM battery solutions that can be deployed at scale and meet the functional requirement of high-power EV charging.
- Use a total-systems approach for battery storage to develop and identify the specific functional requirements for BTMS battery solutions that will provide novel battery systems in the 1–10 MWh range at \$100/kWh installed cost—and able to cycle twice per day, discharging for at least 4 hours, with a lifetime of roughly 20 years or at least 8,000 cycles.

Approach

A cohesive multidisciplinary research effort—involving NREL, INL, SNL, and ORNL—will create a cost-effective, critical-materials-free solution to BTMS by employing a whole-systems approach. The focus of this initiative is to develop innovative battery energy-storage technologies with abundant materials applicable to PV energy generation, building energy-storage systems, EVs, and high-power charging systems. Solutions in the 1–10 MWh range will enable optimal integration of PV generation from a DC-DC connection, increase energy efficiency of buildings, eliminate potential grid impacts of high-power EV charging systems, and lower installation costs and costs to the consumer.

Many lessons learned from EV battery development may be applied to the BTMS program, but the requirements for BTMS systems are unique—carrying their own calendar-life, cycle-life, and cost challenges. For example, EV energy-storage systems need to meet very rigorous energy-density and volume requirements to meet consumer transportation needs. Despite that, current stationary storage systems use batteries designed for EVs due to high volumes that drive down the costs. This creates another market demand for EV batteries, further straining the EV battery supply chain and critical-material demand.

By considering BTMS electrochemical solutions optimized for these applications with less focus on energy density in mass and volume, the potential for novel battery solutions is very appealing. Furthermore, the BOP for a BTMS battery system, or the cost of everything minus the battery cells, is thought to be upwards of 60% of the total energy-storage system cost. In contrast, the EV's BOP costs make up roughly 30% of the total battery cost. Therefore, BTMS will also need to focus on reducing BOP cost through system optimization to realize desired cost targets.

Integration of battery storage with PV generation, energy-efficient buildings, charging stations, and the electric grid will enable new and innovative control strategies. The design parameters are needed to optimize the BTMS system for performance, reliability, resilience, safety, and cost.

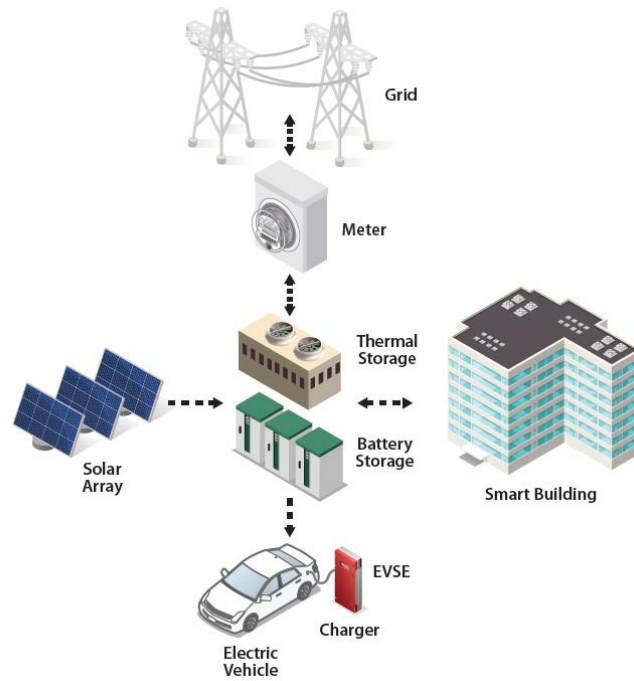


Figure 1. Overview of BTMS relevance.

BTMS Analysis (NREL) – A Summary of FY19 Work

Margaret Mann, Samantha Reese, Tim Remo, Erin Burrell, Madeline Gilleran (NREL)

Background

The goal of the Behind-the-Meter Storage (BTMS) techno-economic analysis conducted in FY19 was to highlight the potential cost barriers and cost advantages that are present when coupling high-demand vehicle-charging loads with different storage configurations. The FY19 cost analysis of BTMS with DC Fast-Charging electric-vehicle supply equipment (EVSE) examined how performance, system utilization, and general changes to the demand profile could affect the minimum sustainable price that an EVSE provider would pass on to their customer.

In FY19, this analysis project focused on a high-level assessment of the potential for BTMS to reduce system costs through avoidance of demand charges. As shown in Figure 1, the system design was limited to charging electric vehicles at a facility similar to that of today's gasoline fueling stations. This report focuses on the results from that work, with a description of the expanded effort beginning in FY20.

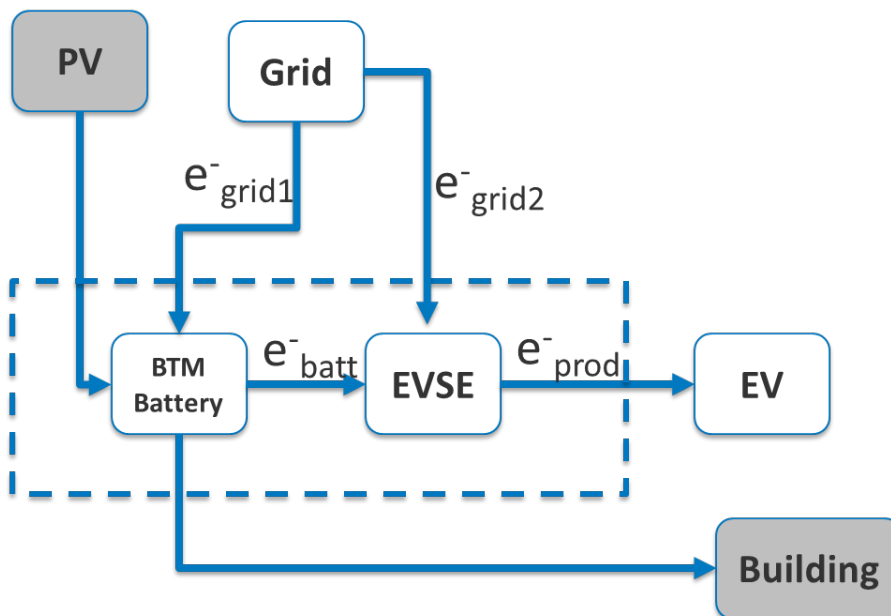


Figure 1. BTMS System Modeled in FY19

Approach

The EVSE/BTMS model was built to incorporate the construction costs, energy load usage scenarios, geographical rate structures, and system financial requirements. The costs over the lifetime of the EVSE facility and equipment are calculated using a standard discounted cash-flow methodology to determine the minimum sustainable price (MSP) for the energy provided to the consumer, denoted as e_{prod} in Figure 1. MSP is the price for which something can sell and pay back all investment and cost within analysis period. The model was designed to be technology- and location-agnostic to allow maximum sensitivity analysis. In calculating the MSP for the electricity (kWh) flowing to the electric vehicle, e_{prod} , the different scenarios investigated included:

- Multiple charging demand scenarios

- Multiple rate structures
- Multiple EVSEs
- Multiple battery sizes.

For this analysis, the general benchmark configuration of a DC fast-charging station was used. The targeted technology milestones and general model assumptions are listed below:

- System
 - 20-year operating lifetime
 - 90% round-trip efficiency
 - Benchmark demand profile
- EVSE Charger Configuration
 - 6 individual charging stalls
 - Rated at 350 kW power
- Behind-the-Meter Storage
 - Li-ion battery pack
 - 5 MWh capacity
 - 90% depth of discharge
 - 1 charge and discharge cycle per day
 - \$209 /kWh battery pack costs

The structure of this model is designed to be technology-agnostic. This allows the comparison of new storage or charging components to be evaluated with respect to the current state-of-the-art designs being installed. It also allows for incorporating other subcomponent cost and construct models into this analysis. An example is the inclusion of the BacPac model developed by Argonne National Laboratory. Changes to the cell designs of the cathode material can have a significant impact on the lifetime performance and cost of a battery cell and pack. These data are computed and imported into the EVSE/BTMS model, which then shows the overall cost effect on the system's total economics.

The model was constructed to incorporate data from the consumer demand behavior, construction costs, and the electrical rate structures to understand the total economic case for the combination of storage with EVSEs.

The Electric Vehicle Infrastructure Projection (EVI-Pro) model was used to obtain a simulated demand profile for charging electric vehicles, assuming DC fast charging at 350 kW. The scenario decided upon was a “gas” station and considered that six chargers would be available. Figure 2 graphically represents the anticipated demand modeled by EVI-Pro for the base scenario.

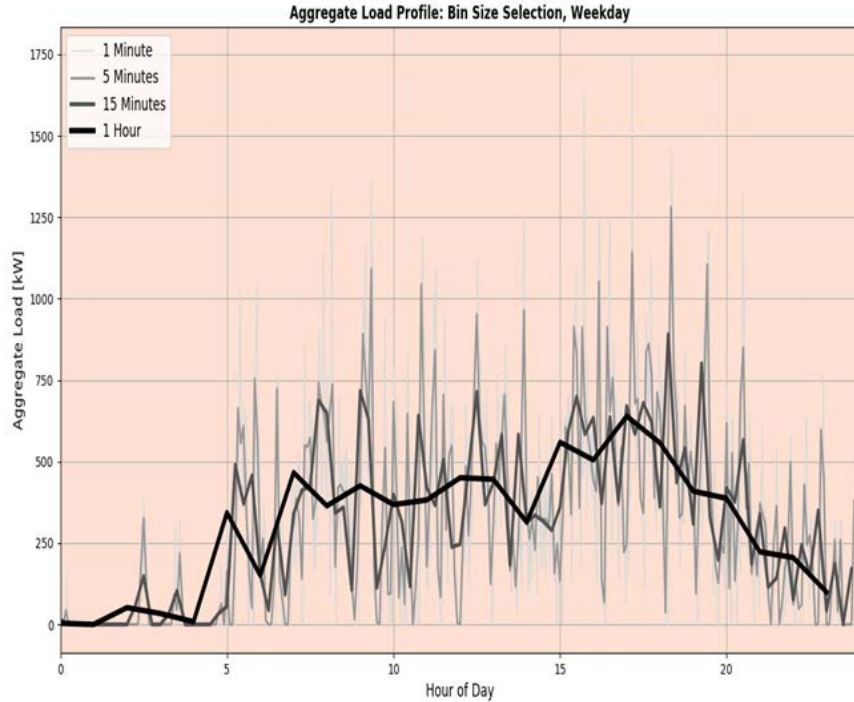


Figure 2. Aggregate demand by time of day for EV charging.

The model was set up to evaluate multiple utility rate structures, made available through the Utility Rate Database (https://openei.org/wiki/Utility_Rate_Database). Two examples of the rates available for Pacific Gas and Electric (PG&E) customers in California are shown in Figure 3.

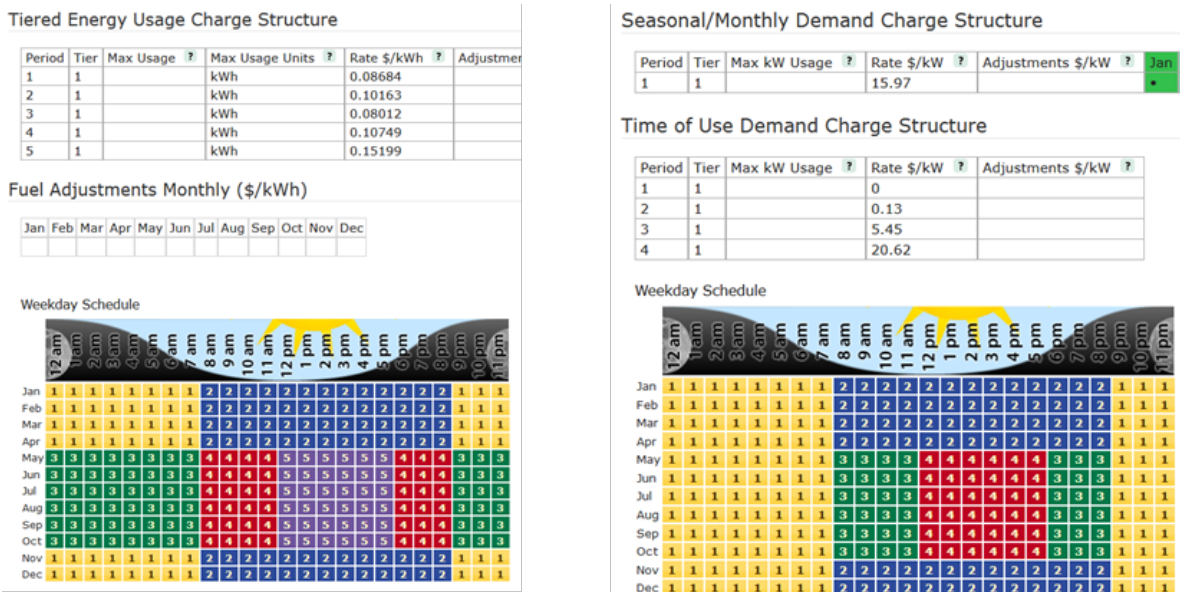
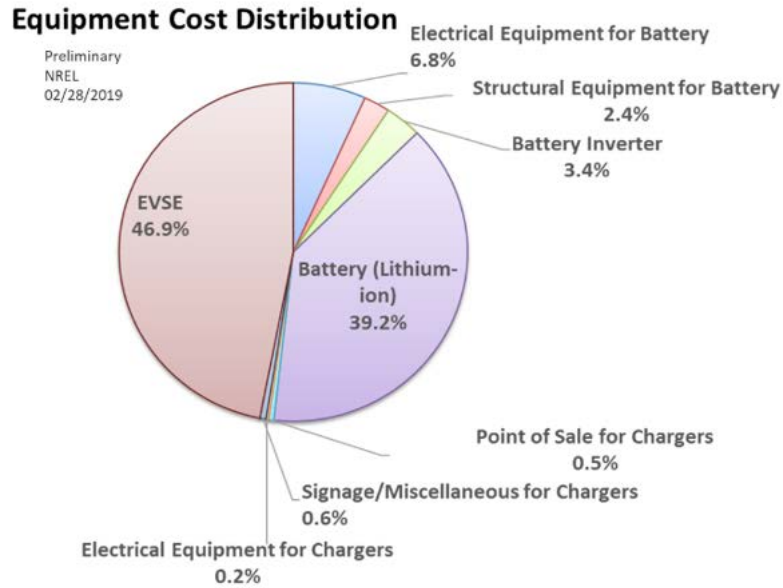


Figure 3. Utility rate structure for PG&E customers, demonstrating the time-variability in electricity price and demand charges.

Results

The distribution of capital costs across the equipment for the EV station with BTMS is shown in Figure 4.

Figure 4. Capital cost for EV charging station with BTMS.



The model assessed the periods of highest demand to determine when to dispatch and charge the battery to minimize electricity cost, including demand charges. The demand for electricity from the grid during these periods was effectively shifted to other periods by using the battery to assist in charging the vehicles. Figure 5 shows the three periods of demand and price change overlaid with the EV demand. The light blue is the original demand; the dark blue shows how that is lowered when the battery is used. Note that in the furthest left quadrant, you can see the increased demand where the battery is charging during the lowest-cost time.

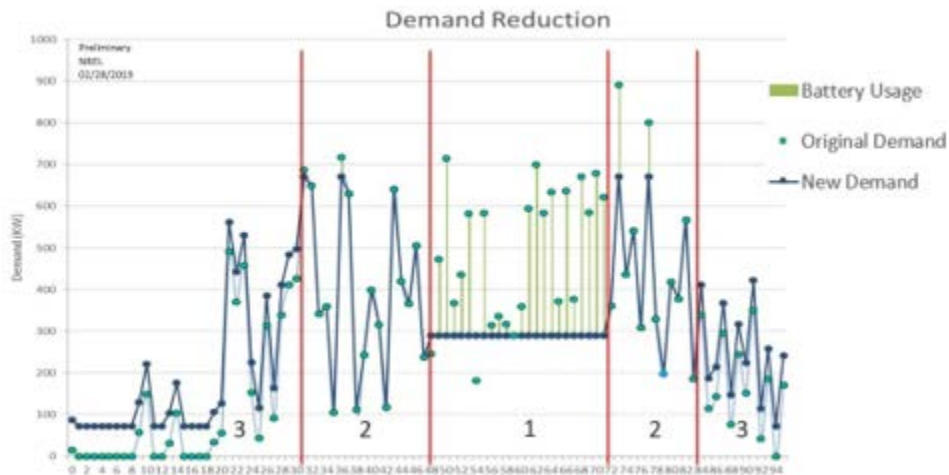


Figure 5. EV charging demand shifting with a behind-the-meter battery.

With current component costs, there is only a small lifetime savings if a battery is used to offset peak demand and electricity cost. But when the battery system achieves the installed target cost, a ~40% lifetime savings would be achieved.

The initial costs for BTMS systems can be offset over time through reductions in the station’s total electricity costs. The reductions are primarily through lowering demand charges, with the secondary effect of shifting electricity usages from peak to off peak times.

Reductions in peak times can offset demand charges and keep the cost for the end consumer relatively flat over the life of the system. A closer look at the rate structures show that the most impactful BTMS systems involve fewer high demand intervals followed by a low baseline energy consumption. An extreme case is highlighted in Table 1, where the energy consumption is the same as our current baseline scenario, but the demand spike is depicted for a worst-case scenario.

Table 1. Cost data for extreme demand scenario

	Summer			
Standard Scenario (Monthly Values)	EVSE Only		EVSE+BTMS	
Fixed Charge (Total)	\$ 1,499	1%	\$ 1,499	5%
Energy Charge (Total)	\$ 25,112	9%	\$ 23,131	7 8%
Demand Charge (Period 1)	\$ 246,986	90%	\$ 3,815	13%
Demand Charge (Period 2)	\$ 1,008	0%	\$ 1,008	3%
Demand Charge (Period 3)	\$ 24	0%	\$ 59	0%

Demand Charge (Total)	\$ 248,019	90%	\$ 4,882	17%
Total Monthly Charge	\$ 274,629	100%	\$ 29,511	100%
Cost of Electricity from Grid (\$/kWh)	\$ 1.2221		\$ 0.1245	
MSP	\$ 1.5911		\$ 0.2779	

Systems that operate under highly variable demand loads scattered throughout a daily operation, with a high average energy baseline load, require larger battery systems to impactfully reduce the total MSP. These systems can still be economically viable over the life of the system, but the high cost of the battery pack will cause a longer payback period. This leads to concerns of longer system reliability requirements. Another important aspect to properly size a BTMS storage system involves optimizing the ration of demand charge to energy charge. Future analysis will also incorporate on-site distributed generation, which will have the potential to reduce the energy charges as well as further assist to reduce demand.

Seasonal charges will also contribute to how the battery will operate. In some cases, standby or use as a backup system may extend the life of the system. This is due, in part, to demand charges that only exist during the four- to six-month summer periods. Table 2 shows one example of the large potential price difference in seasonal operations. As these systems become more standardized, there is even the possibility that containerized systems could be considered mobile assets and moved from one location of value to another location of higher value once or multiple times during its lifetime based on system economics. This would allow for more, shorter positive payback periods over the asset’s usable life.

Table 2. Cost data for seasonal demand scenario

Standard Scenario (Monthly Values)	Off Summer				Summer			
	EVSE Only		EVSE+BTMS		EVSE Only		EVSE+BTMS	
Fixed Charge (Total)	\$ 1,499	4%	\$ 1,499	5%	\$ 1,499	3%	\$ 1,499	6%
Energy Charge (Total)	\$ 20,451	61%	\$ 20,588	74%	\$ 24,273	53%	\$ 20,136	86%
Demand Charge (Period 1)	\$ 11,407	34%	\$ 5,799	21%	\$ 14,729	32%	\$ -	0%
Demand Charge (Period 2)	\$ -	0%	\$ -	0%	\$ 4,854	11%	\$ 1,680	7%
Demand Charge (Period 3)	\$ -	0%	\$ -	0%	\$ 89	0%	\$ 135	1%
Demand Charge (Total)	\$ 11,407	34%	\$ 5,799	21%	\$ 19,672	43%	\$ 1,816	8%
Total Monthly Charge	\$ 33,357	100%	\$ 27,886	100%	\$ 45,444	100%	\$ 23,451	100%
Cost of Electricity from Grid (\$/kwh)	\$ 0.1484		\$ 0.0932		\$ 0.2022		\$ 0.0989	
MSP	\$ 0.3061		\$ 0.2409		\$ 0.3696		\$ 0.2477	

One potential driver for a mobile system would be changes in the demand profile during the system's lifetime. A system that is oversized for current demand results in a large price penalty to the consumer and operator. This will be a challenge for EVSE+BTMS systems designs. The price penalty for not installing a BTMS system is severe due to potential high demand charges and grid upgrade costs that can be incurred with site construction. Oversizing a system, however, can create an upfront potential barrier to market adoption.

BTMS coupled with high demand rates and irregular demand profiles can have a positive rate of return when systems have a long operational life. The current specified system lifetimes under 10 years do fall short of a positive return. But given the ability to upgrade and extend the life of a system, a simple business model as described for this analysis is likely to change over the full operating life span. These changes could include repowering or expanding the system capacity. Given the falling cost of batteries packs and typical rising inflation values, designing a system capable of expansion in a plug-and-play fashion could provide a greater economic benefit because there could be advantages specific to permitting and soft costs. The current bottom-up analysis for systems designs shows that the battery pack itself is around 50% of the total system capital cost.

It is also important to understand how the energy rate structures may change over time given the emergence of low-cost energy from distributed generation and changing energy load profiles. Energy storage has the ability to operate under multiple use-cases, but the largest attraction to energy storage is the energy arbitrage operation of operating low-cost energy from one timeframe and dispatching the energy at expensive rate timeframes. In doing so, energy storage does not generate energy but rather shifts it from one time to another so that all energy storage systems require some generation source—whether that is the grid or distributed generation sources such as renewables. BTMS systems can smooth the operational demand for a load profile, potentially reducing demand spikes on a transmission line. This may reduce the costs of upgrading transmission and distribution systems and—of particular benefit to EV station owners—reduce the cost of interconnecting their systems to the grid. Future work should examine a wide range of current and predicted utility rate structures, as well as grid interconnection costs, to better understand how BTMS systems should be defined to optimize cost.

Conclusions

The rate structure, load profile, and system operating capacity are three of the most significant drivers to optimizing the BTMS system configuration and therefore to planning for the lowest MSP value. DC fast charging without storage has the potential to significantly increase the customer's average MSP for electricity by an order of magnitude. But simply adding storage will not reduce the cost back into 0.10–0.20 \$/kWh range. This is because the capital cost for these storage systems is significant between 300–500 \$/kWh. Research advances to reduce battery cell and balance-of-system costs can reduce the upfront costs for BTMS with EVSE.

BTMS by itself can significantly impact demand charges, but in general it will have only a small impact on shifting the energy charges. Adding distributed generation with renewables could future reduce long-term energy costs for the consumer by not only shifting electricity rates from peak to off-peak timeframes, but also, by reducing the total amount of energy pulled from the grid.

The results of this analysis show that BTMS coupled with DC fast-charging EVSE can be cost-effective today with long lifetime and high system reliability. The challenge for these assets will be how these systems will operate over their usable lifetimes and if they can achieve long life in the field. Asset operations will be influenced by changes to EVSE demand and market growth. Utility rate structure is also likely to change over time, which will impact this marketplace. Designing systems that are easily scalable, portable, and upgradeable have the potential to provide long-term profitability for these assets.

FY20 Work Plan

Electric-vehicle adoption is expected to grow significantly over the coming years, and it could have a significant and potentially negative effect on grid infrastructure. Additionally, the rapid penetration of solar photovoltaic generation installed on buildings is leading to new challenges for the electric grid. In response to the potentially large and irregular demand from EVs, along with changing load profiles from buildings with on-site generation, utilities are evaluating multiple options for managing dynamic loads, including time-of-use pricing, demand charges, battery storage, and curtailment of variable generation. Buildings, as well as commercial, public, and workplace EV charging operations, can use energy storage (e.g., batteries, thermal energy storage) coupled with on-site generation to manage energy costs as well as provide resiliency and reliability for EV charging and building energy loads.

The key question this project will be examining starting in FY20 is: What are the optimal system designs and energy flows for thermal and electrochemical BTMS with on-site PV generation enabling fast EV charging for three variables: climate, building type, and utility rate structure?

The previous effort created a framework for evaluating a multi-component BTMS system; however, additional work is needed to fully include and analyze on-site generation, thermal storage, building interactions, and possible energy export. This project seeks to integrate into a single interface the existing models and knowledge about PV generation, building energy use, battery storage, thermal energy storage, and EV charging. This combined framework, referred to as **EnStore** for Energy Storage, will be scalable and flexible, and it will answer questions about the tradeoffs between battery and thermal energy storage size, energy storage dispatch, PV size, EV charging demand, building energy demand, and use of grid energy. EnStore will be designed as a system optimization model, focused on the following metrics:

- Levelized cost of ownership (LCO) (also known as MSP, levelized cost of energy (LCOE), and profited cost; related to payback period and return on investment (ROI)) to the system owner, including Beyond LCOE project implications.
- Total system energy use (efficiency) to meet varied energy demands from the building and EV charging.
- Resiliency in terms of grid backup time (duration for supporting 100% of the loads and critical loads).
- Quantified daily load flexibility, both in terms of power and energy.

The building type and design will be the foundation for the overall system configuration, because building use is the determining factor for how people access energy, now and in the future. PV installation on the building and the addition of EV charging at the building site will be included in the configurations examined. For building energy use, the model will include representative cities for the ASHRAE climate zones. Several building types to be assessed will include the following:

- Retail big-box grocery store
- Commercial office building
- Fleet vehicle depot and operations facility
- Multi-family residential
- EV charging station (with multiple EVSEs, as determined by load projections).

For each building type, the scenarios to be evaluated include:

- A. Solar energy
 - i. PV generation
 - ii. No PV generation
 - iii. Selling electricity to the grid (net metering)
- B. Energy storage
 - i. Battery
 - ii. Thermal
 - iii. Battery and thermal
 - iv. No energy storage
- C. EV charging
 - i. 1, 6, 12 EVSEs, extreme fast charging and/or Level II charging, depending on building type and load projections
 - ii. No EV charging
- D. Rate structure
 - i. Flat rate structure
 - ii. Variable demand charges (in both threshold and cost multiplier)
 - iii. Time-of-use (TOU) structures: both high and low ratios between on- and off-peak rates
 - iv. Net metering at both retail and bulk rates should be considered for all the preceding rate-case scenarios.

The integrated EnStore modeling framework will provide critical information to several stakeholders, such as DOE decision makers, utilities, industry players investing in EV charging, PV, and others, while avoiding duplication and divergent approaches for evaluating BTM energy storage. This model will be able to answer the following types of questions, and others related to BTMS:

Priority Questions:

1. What is the sensitivity of analysis results to the variability of location, building loads, EV charging demands, and component costs, and combinations of each case within those categories?
2. What research achievements (e.g., material characteristics for thermal energy storage, battery material costs and lifetime, PV deployment) would increase the economic viability of the various configurations of BTMS at multiple locations?
3. What level of improved iterative feedback modeling, informed by BTO research on battery and thermal energy storage systems, would be necessary to optimize sizing and designs for subsystem components (PV, battery size and operation, thermal storage)?
4. What is the potential energy savings, PV energy generation, and EV demand coverage in different locations across the United States, as a function of technical and cost improvements?

Electrical and Thermal Design Behind the Meter System (Oak Ridge National Lab)

Contributors (Oak Ridge National Lab) [Madhu Chinthavali, Pankaj Bhowmik]

Project Objective: Installation-oriented electrical and thermal design of a behind-the-meter system involving battery-based electrical energy storage system (EESS), thermal energy storage, building load, and extreme fast-charger-based electric vehicle supply equipment (EVSE)

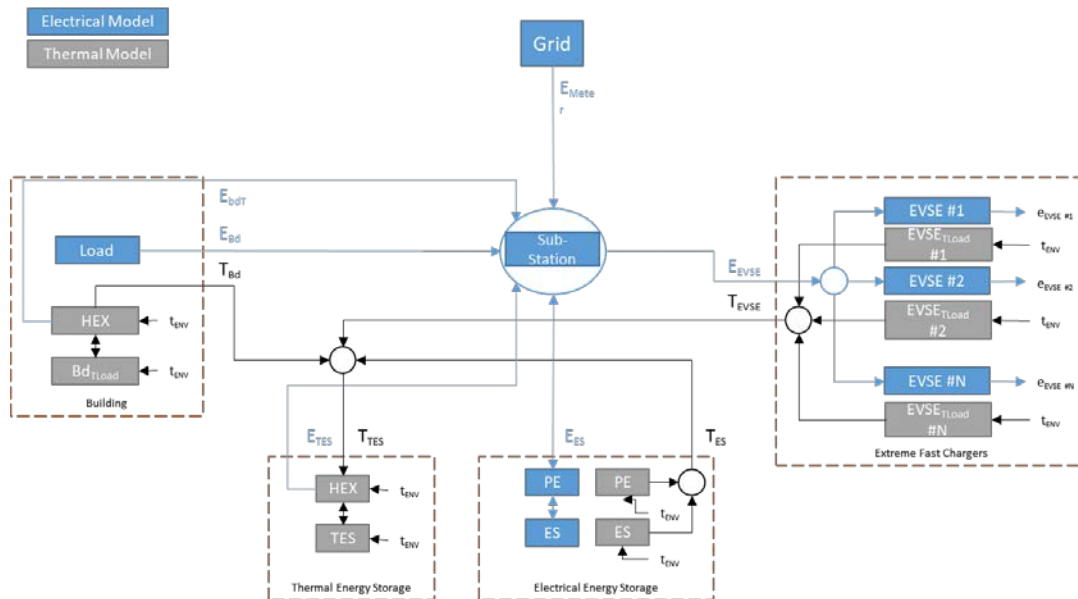


Figure 1. Block schematic based on signal flow graph representing the overall electrical and thermal model for the entire system.

Q2 Challenges

- ✓ Installation-oriented design of battery energy storage system (BESS)
- ✓ Pricing estimate of BESS
- ✓ Thermal-loss estimate of BESS

Q3 Challenges

- ✓ Installation-oriented design of electric vehicle supply equipment (EVSE)
- ✓ Pricing estimate of EVSE

Background

An installation-oriented design of an EVSE may be subdivided into two major design items, as follows:

1. Electric vehicle (EV) load
2. Power electronics (PE)

This report discusses the design of the PE that has to be installed to supply power to an EV load from the grid. The design of PE has certain aspects that must be performed alongside determining the nature of EV load. Here, we consider EV extra-fast-charging stations. These installation design aspects are also reviewed here. We also present an estimate of the costs and losses associated with the design of an EVSE.

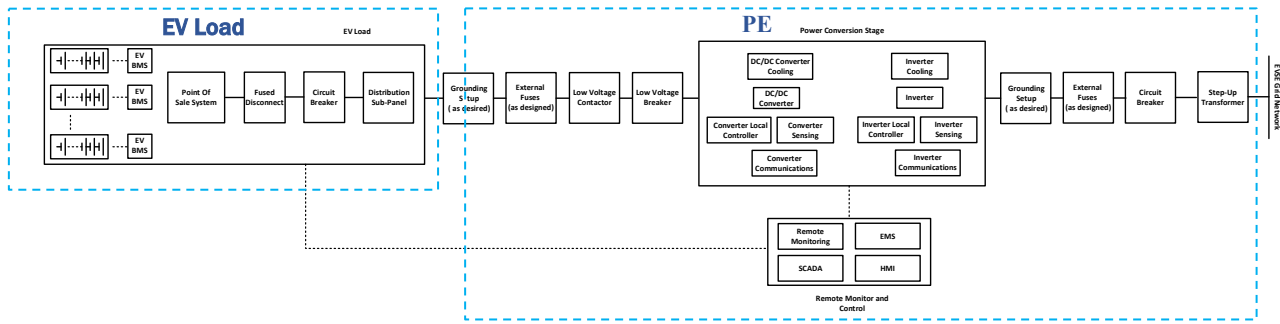


Figure 2. Block schematic of an electric vehicle supply equipment.

A simplified block schematic of a typical EVSE installation with EV load and PE is shown in Figure 2. PE consists of three main aspects from the perspective of electrical power flow and signals:

- a. Control and Protection
- b. Power conversion
- c. communications

Protection may be further subdivided into DC-side and AC-side protection. Typically, both DC- and AC-side protection involve fuses, contactors, circuit breakers, and proper grounding setup. Also, a step-up transformer is added while integrating the PE to the grid, and to step up the voltage, an additional level of isolation is added to EVSE from the utility grid. Depending on the number of EVs that can be simultaneously charged, the protection design costs and losses will vary.

Power conversion incorporates the power converter, power converter cooling system, power converter sensing, and connecting cables. The designed PE system may be rated at 1 MVA power-handling capacity. But the estimated range for costs presented in this chapter may be used to evaluate PE designs up to 100 MVA.

Control and communications includes the converter controller, converter communications, remote monitoring, supervisory control, and data acquisition, EV load battery communication system, and human/machine user interface for the point-of-sale (POS) system. This element of a PE design is also responsible for the control and coordination between EV load, DC and AC protection devices, and power conversion system.

These aspects of a PE design only demonstrate the electrical power flow, signal monitoring, control, and protection perspective. To view the site installation-oriented design flow of a PE system, the various aspects such as site allocation, site building, engineering construction, labor, and costs, to name a few, have to be incorporated into the design. This particular commercial installation-oriented design will provide more insight into cost estimate and loss estimate for any proposed EVSE. The next section discusses this design flow for an EVSE system. The design considerations that will be used to estimate the costs and losses for an EVSE are presented in Table 1.

Table 1. Design considerations for cost and thermal model of an EVSE

Parameters	Values	Units
DC Bus Voltage	1,500	V
DC Bus Current	1,000	A
DC Bus Power	1.5	MW

AC Bus Line Voltage	480	V
AC Bus Current	1,200	A
AC Bus Active Power	1	MW
Grid Line Voltage	13.8	kV

Installation-Oriented Design of Electric Vehicle Supply Equipment

The installation-oriented design for an EVSE is subcategorized into five main elements:

1. Power conversion system (PCS)
2. Structural balance of system (SBOS)
3. Electrical balance of system (EBOS)
4. Engineering procurement and construction (EPC)
5. Soft cost

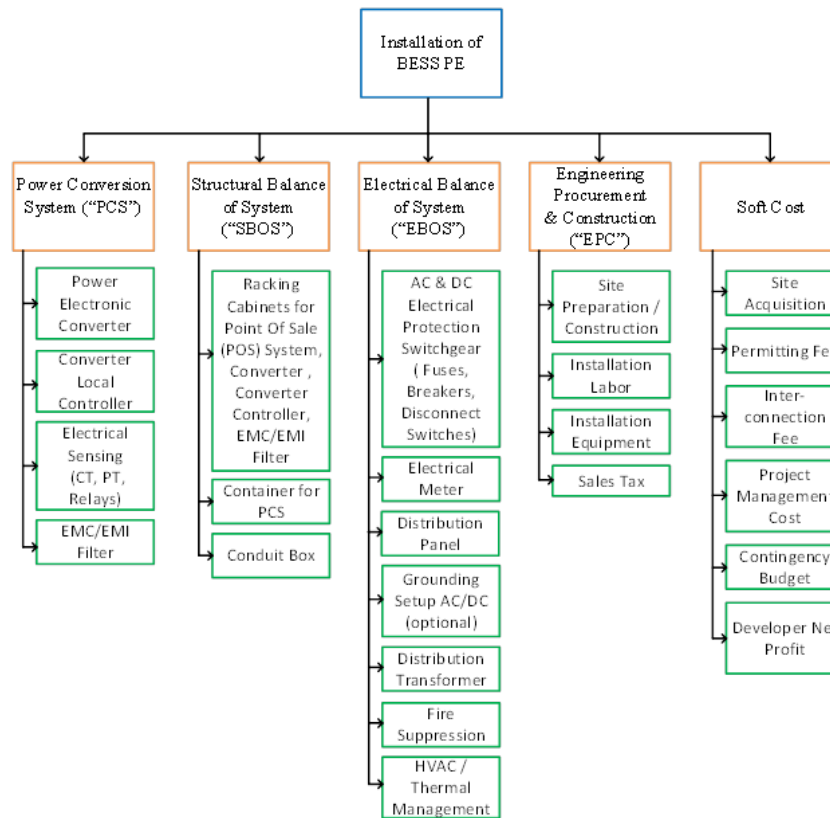


Figure 3. Block-tree-type categorization of the various aspects of installation-oriented design of EVSE [1–5].

The PCS involves procuring the converter, converter local controller, electrical sensing equipment such as the current transformer (CT), potential transformer (PT) and relays, and also the EMI/EMC filter. This category has been so named because it involves conversion of the AC power obtained from the grid to DC power that is being supplied to the EV load.

The SBOS involves procuring all the components that provide structural integrity and housing to install the PCS as well as EBOS. It involves racking cabinets for the POS system, converter, converter controller, and EMC/EMI filter. It also incorporates the container for housing the PCS and conduit boxes to house the cable terminal connections.

The EBOS involves procuring all the components that monitor electrical power flow and signals and that under fault conditions protects the PCS, EV load, and grid. It also provides added functionality of fire suppression and management of the thermal energy dissipated from the PCS through HVAC or other cooling technologies. It involves AC and DC components such as fuses, breakers, meters, and disconnect switches. It also includes a distribution transformer for isolation as well as voltage step-up purposes. In the case where no grounding is available in the PCS, a grounding setup on the DC or AC side may be considered to provide a return path to fault current or neutral current under fault or unbalanced system conditions.

EPC is a multi-faceted and human-resource intensive activity that is crucial to installing an EVSE PE. It involves preparing and constructing a site for the installation of PCS, SBOS, and EBOS. It also involves acquiring or renting equipment for installing PCS, SBOS, and EBOS. To perform all these activities in EPC, installation labor has to be hired with wages whose minimal value may vary from state to state. Most importantly, all the taxes levied on this overall EVSE installation process are included under sales tax, which may again vary by state.

Lastly, soft cost entails acquiring the site for EVSE installation, permitting fee for permission to install EVSE, interconnection fee for EVSE interconnection with the utility grid, project management cost for planning and executing the project for installation of EVSE, and the overall developer net profit generated by undertaking the EVSE installation.

Pricing Estimate of Electric Vehicle Supply Equipment

Table 2 lists the EVSE PE installation components and presents the estimated rates for each process as a range in the units of U.S. dollars per watt (\$/W). The total estimated cost is also estimated from the rates based on the power rating of 1 MW.

Table 2. EVSE component-wise cost estimate for a 1-MW, 13.8-kV setup [1–5]

EVSE Installation Components	Estimated Rate (\$/W)	Estimated Total Cost (\$)
PCS	0.11–0.16	110,000–160,000
SBOS	0.07–0.12	70,000–120,000
EBOS	0.10–0.20	100,000–200,000
EPC	0.12–0.34	120,000–340,000
Soft Cost	0.08–0.19	80,000–190,000

Table 3 lists the complete EVSE installation total estimated rate in \$/W units, which is the summation of each component rate from Table 2. The total estimated cost is then calculated from the total estimated cost based on the power rating of 1 MW.

Table 3. EVSE PE total cost estimate for a 1-MW, 13.8-kV setup [1–5]

Cost Estimate for a 1-MW, 13.8-kVac Setup:		
Total EVSE Installation	Total Estimated Rate (\$/W)	Total Estimated Cost (\$)

0.48–1.01

480,000–1,010,000

Conclusions

The key lessons learned from completing this quarter's project milestones are summarized as follows:

- Design of an EVSE depends much on the EV load being served.
- Installation-oriented design requires a proper understanding of the three main aspects of the entire system: protection, power conversion, control and communications.
- Pricing estimation of an EVSE has been discussed in detail in the report, and it may be seen that the estimated total cost rate, \$/W, varies greatly as the EPC and soft cost have a much greater difference between the minimum and maximum rates. It is so because these design elements contain aspects that are governed by financial constraints that vary by state, by area (location of site), or by required human resources.

References

- [1] <https://smartchargeamerica.com/electric-car-chargers/commercial/chargepoint-express-250/>
- [2] https://afdc.energy.gov/files/u/publication/evse_cost_report_2015.pdf
- [3] <https://www.epri.com/#/pages/product/000000003002000577/?lang=en-US>
- [4] <https://www.ohmhomenow.com/electric-vehicles/electric-vehicle-charging-stations-business/>
- [5] <https://avt.inl.gov/sites/default/files/pdf/arra/PluggedInSummaryReport.pdf>

BTMS Testing Section

Contributors: INL, SNL, NREL

Background

Testing activities in the first year of the program focused on several aspects of forming testing protocols to assess the gaps in performance of different battery chemistries relative to the high-level BTMS targets that were established at the program's onset. First, we performed an initial review of legacy life data from vehicle-systems energy storage testing. Next, put together preliminary testing protocols to begin cycling a few types of cells under both a single simplified use-case and under a small matrix of varied thermal and depth-of-discharge conditions that generally affect aging. We evaluated these early data along with the legacy data to aid in further testing protocol development that focused on better accelerated test methods, enhanced with machine-learning techniques, and we refined application-specific cycling protocols and performance tests.

Results

Legacy data review looked at both cobalt-free cell chemistries and some with cobalt-bearing cathode materials, in addition to published life and performance data. From 2010–2012, two builds of lithium iron phosphate (LFP)-graphite cells were cycled and aged under test protocols developed for EVs at 30°C. The later build reached 20% capacity fade before 1,500 full-DOD cycles were reached.

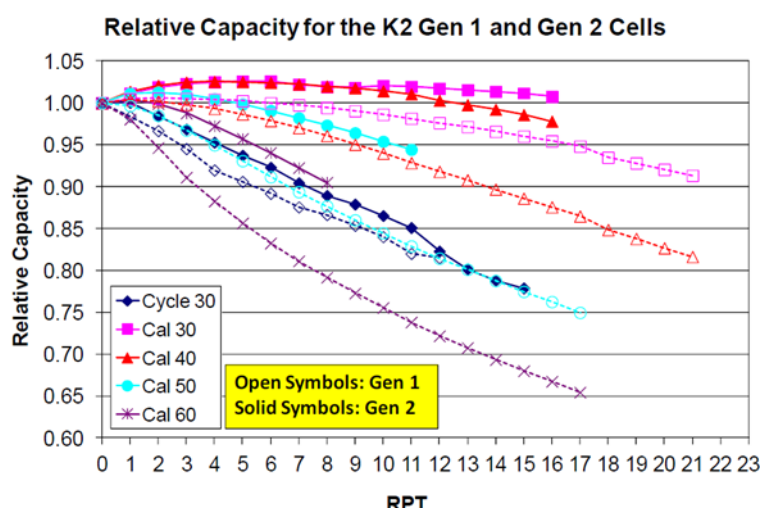


Figure 1. Capacity data throughout life testing is shown for LFP/graphite EV cells DST cycled to full depth of discharge.

LFP cells with lithium titanate oxide (LTO) anodes were reported to have extremely long cycle life, due in part to the lack of solid-electrolyte-interphase formation on the anode. Testing from 2012–2013 with continuous cycling at 30°C yielded less than 6,000 1C/1C full cycles to 20% capacity fade. This did not align with the developer's testing data at the same ambient temperature, but much higher rates, using a 5C/10C cycling protocol, which yielded 20,000 cycles without appreciable fade. This specific couple is not known as being pursued because of its very low energy density, although LTO anodes are generally capable of long cycle life.

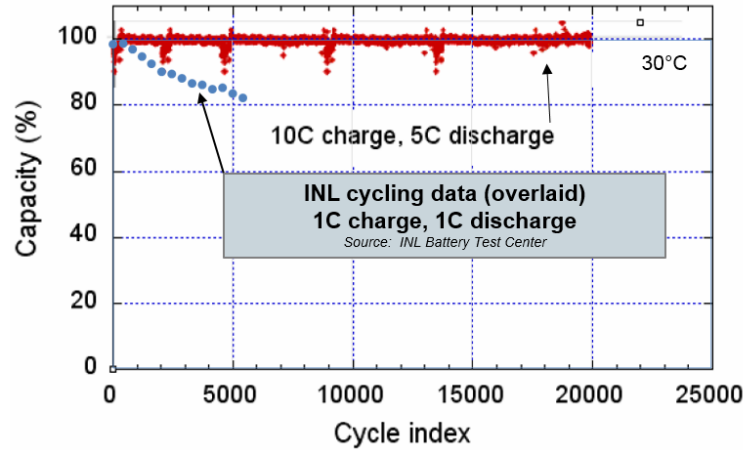
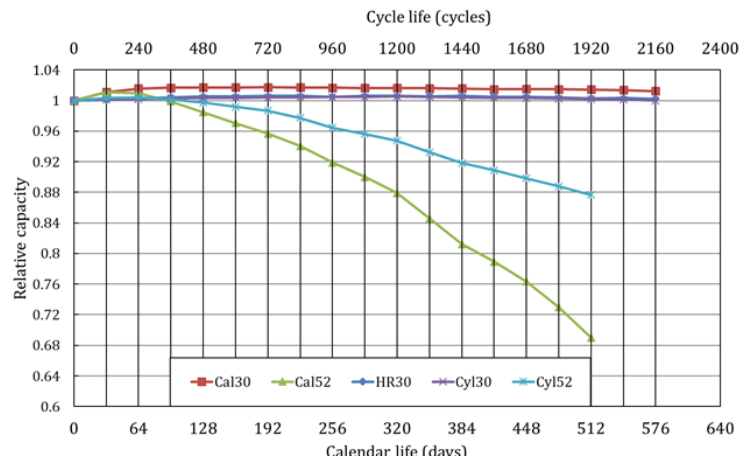


Figure 2. INL cycling data at 1C/1C is shown overlaid on 5C/10C cycling data published by the developer.

Another LTO-anode cell type, with an unspecified cathode thought to be LMO with NMC, was cycled under test protocols developed for EVs at 30°C and 52°C from 2016–2018. These prismatic cells showed no fade under DST cycling with both C/3 slow-charging and 5C fast-charging after more than 2,000 cycles. High temperature rapidly accelerates these cells’ capacity loss, and that is compounded by rest at 100% SOC, as evidenced by the high fade rates of the calendar-life cells at 52°C.

Figure 3. Calendar- and cycle-life data for LMO-NMC/LTO cells.



Early Nissan Leaf LMO/graphite EV cells, manufactured by AESC, were cycled at three different temperatures. The cells were cycled using an EV DST discharge profile, from 90% SOC, removing 60% of the total BOL energy. Recharge was done using a constant-power, constant-voltage protocol approximating a slow C/7 charge. Temperature had a primary impact on the rate of capacity loss of these cells. Because the primary purpose of this testing was to investigate the effects of charging rate on degradation, the testing was stopped after 864 cycles. Linear extrapolation of the last six 30°C data points yields an approximation of 2,100 of these 60% DOD cycles to 80% capacity remaining. Incremental capacity analysis indicated capacity loss due mainly to loss of lithium inventory and loss of active material on the anode for all three temperature conditions.

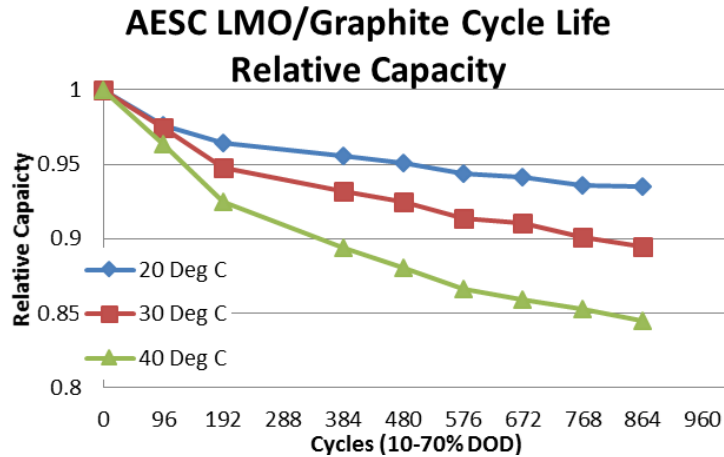


Figure 4. Cycle-life data for LMO/graphite cells.

NMC-LMO/graphite pouch cells were cycled from 2016–2019 under a plug-in hybrid EV (PHEV) charge-depleting cycling protocol from 90% SOC, removing 65% of their total energy per cycle, at 30°C. These cells retained 78.5% of their original capacity after more than 5,000 PHEV-40 CD cycles.

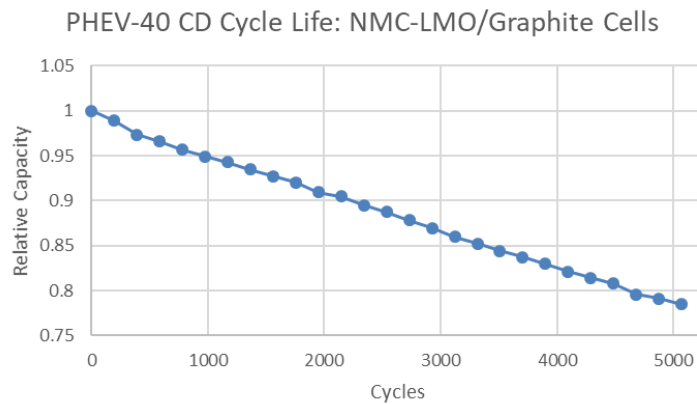
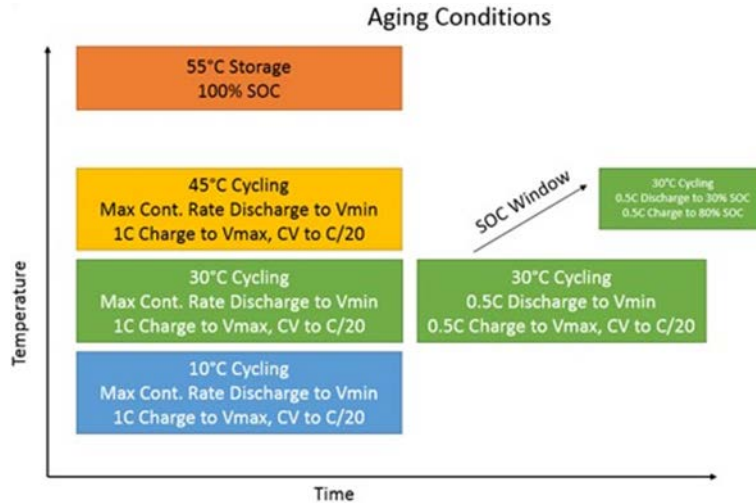


Figure 5. Cycle-life data for NMC-LMO/graphite cells.

The BTMS program specified investigation of 1–10 MWh storage systems used to support extreme fast-charging (XFC), among other co-beneficial systems including buildings electrical and thermal needs and on-site renewable electricity generation. Although complex use-cases were being discussed and developed, we selected a gas-station-like model featuring six 350-kW DC fast-chargers with 1 MWh of storage as a scenario to base initial battery rate requirements for a preliminary cycle-life protocol. Pairing the minimum energy storage system size with six XFC units that concurrently use 100% of their power from the energy storage system yields about a 2:1 power-to-energy ratio system requirement, which can be approximated by a 2C discharge of a cell. This situation could be realized when all of the energy supplied to XFC units is supplied from the BTMS system, accomplishing a full load shift of off-peak energy. It is likely that in many scenarios, simultaneous use of all XFC stations would be occasional, and XFC power would be supplied by both the grid and the BTMS system. In this case, a lower rate would be realized. A C/2 rate was chosen as a more moderate discharge rate for preliminary cycling based on discussion of these factors. This rate results in less than 6 full cycles per day, when accounting for CV charging time. High discharge rates, within cell manufacturer specifications and laboratory channel resource availability, were chosen to accompany the slow cycling, to accumulate cycles more rapidly and to accelerate capacity loss. Aside from a 30°C reference condition, 10°C and 45°C were also chosen to affect rates of capacity loss. Finally, some cells were cycled shallowly, within

the middle 50% of their capacity, to investigate path dependence of capacity loss. We selected NMC/graphite, NMC/LTO, and LFP/graphite commercial cells with quick availability.

Figure 6. Preliminary test matrix for cells with 6-XFC and 1 MWh ESS and accelerated aging conditions



Sandia National Laboratories assembled a pack-estimating table (Table 1), and this calculation demonstrated that lowering the applied current of the string can be cost prohibitive due to the number of cells needed and the implied balance of plant. What resulted from this discussion was a test plan that spanned a variety of use cases—from pushing the limits of the cells to standard cycling—to fully understand the capabilities of the cells and their aging characteristics.

Table 1. Pack estimation calculation table, where the shaded row represents the C/2 discharge rate.

Current Applied per String	Current in C rate (assuming 3.5 Ahr)	Capacity consumed	Minimum number of strings	D-Rated Voltage	Minimum Cells in String	Recommended Cells in String	Pack Power (Without Power Electronics)	Total Number of Cells	COST? (k)
50	14.29	12.5	19.4	2.8	125	138	0.374	2671	10.7
40	11.43	10	24.3	2.9	121	133	0.374	3224	12.9
30	8.57	7.5	32.4	2.95	119	131	0.374	4226	16.9
20	5.71	5	48.6	3	117	128	0.374	6233	24.9
10	2.86	2.5	97.1	3.2	109	120	0.374	11688	46.8
5	1.43	1.25	194.3	3.3	106	117	0.374	22667	90.7
1.75	0.50	0.4375	555.1	3.32	105	116	0.374	64372	257.5
1	0.29	0.25	971.4	3.35	104	115	0.374	111642	446.6

The 2-hour discharge capacity and pulse-power capability of each cell was measured monthly in a reference performance test. Every third performance test included a set of 20-hour charge and discharge cycles that can be analyzed to understand differences in aging mechanisms among test conditions, in addition to the characterization of performance loss through time and cycling. Cells were fixtured and placed in thermal

chambers and connected to cycling equipment, and baseline testing and life cycling and aging commenced in Q2. Initial results showed cell-level energy densities of 485 Wh/L for the NMC/graphite cells, 133 Wh/L for the NMC/LTO cells, and 98–107 Wh/L for the LFP/graphite cells, for power and energy application types, respectively.

The NMC/graphite cells suffered rapid degradation in the first set of cycle aging, and the rate of capacity loss generally increased with increasing charge and discharge rates. Only the cells in the slowest 2-hour charge and 2-hour discharge cycling condition retained enough capacity to complete the first and second reference tests. The NMC/graphite cells in the other cycling conditions, including up to 1C charge and 1C discharge, lost more than 25% capacity before RPT1. The results from the cells tested through the third reference performance test are shown in the figures below. The shallow-cycled cells show little benefit relative to the cells cycled over the entire SOC window.

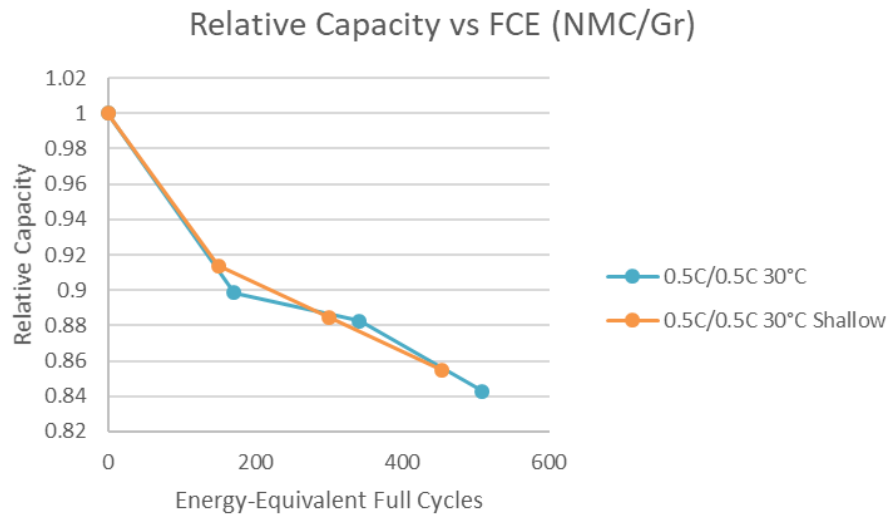


Figure 7. Cycle-life testing results for the NMC/graphite cells.

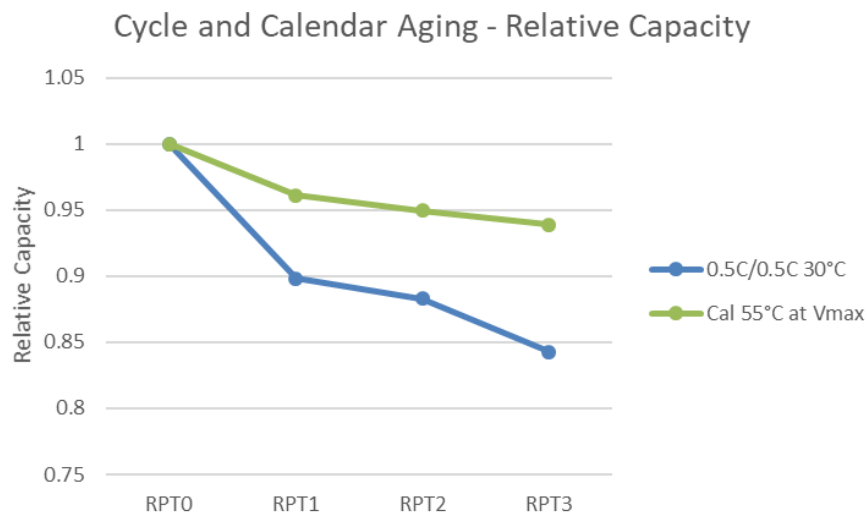


Figure 8. Calendar testing results for the NMC/Graphite cells, shown with the baseline cycling condition results.

The NMC/LTO cells had a maximum continuous discharge rate of 6C, and that condition was applied, along with 1C and C/2 cycling conditions. Only the colder cycling condition showed significant fade at the second RPT. Due to the different rates and different temperatures, varying amounts of capacity were discharged from each test condition, resulting in disparate numbers of cycles per time period. These data are shown in Figure 9, plotted relative to the full-cycle equivalent (FCE) of cumulative energy discharged at the 30°C, 2-hour discharge reference condition. These cells have shown less than 1% fade over more than 1,700 cycles at slow- and high-rate discharge and at both 30°C and 45°C conditions. The cycle-by-cycle discharge capacity for each condition is shown as well in Figure 10. However, note that the cycle count is raw, and each cycle at the various conditions are not equivalent due to rate and temperature.

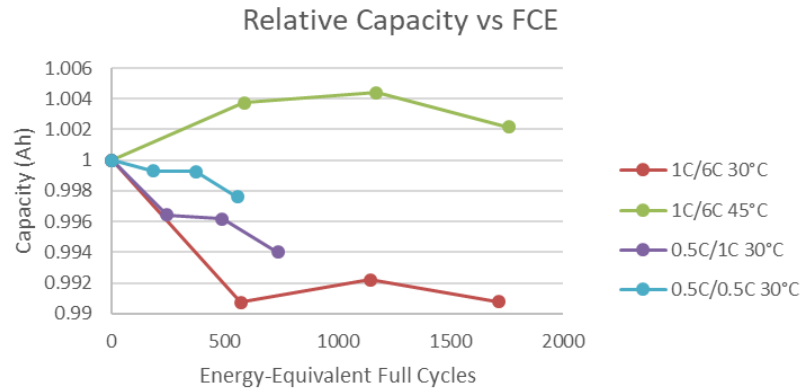


Figure 9. Cycle-testing reference-performance-test (RPT) capacity results for the NMC/LTO cells.

Two different cell constructions are currently being investigated for the LFP/graphite system. These cells have undergone close to 130 consecutive days of continuous cycling. The effects of this cycling on the capacity fade of the cells can be observed in Figure 11. Results show that on average the power cells have lost ~10% whereas the energy cells have lost close to ~30% in the worst case. It is difficult to say that the ~30% loss in the energy cell is representative without additional cells to provide statistics. Differences in the state-of-health testing of these cells can also be observed as demonstrated in Figure 12.

Capacity Retention of LFP/Graphite Cells Cycled at 30°C

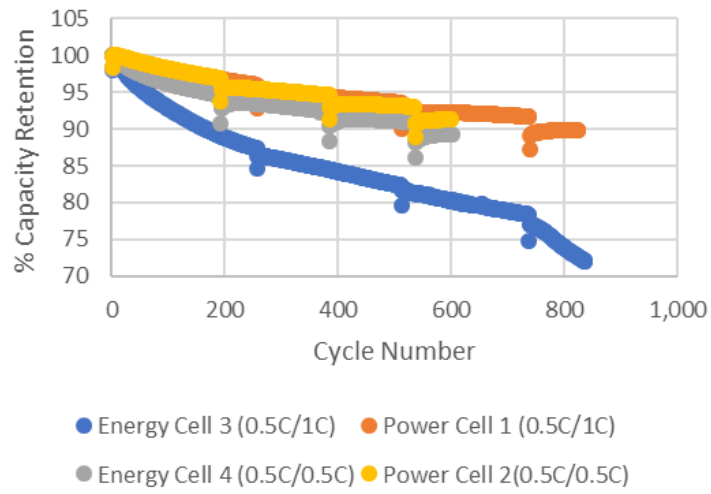


Figure 10. Cycle-by-cycle testing capacity results for each cycling condition for the NMC/LTO cells.

NMC/LTO Raw Cycle-Life Capacity

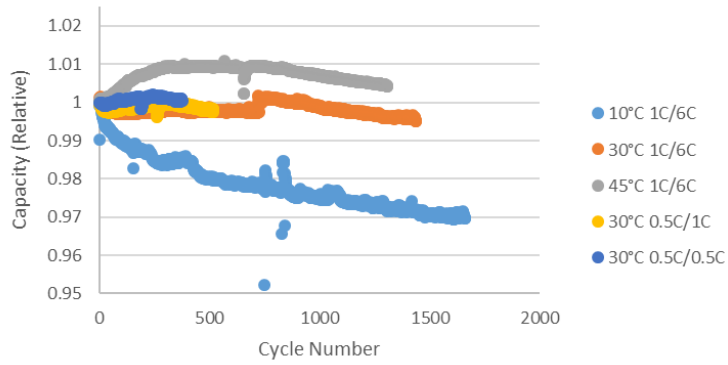


Figure 10. Cycle-by-cycle testing capacity results for each cycling condition for the NMC/LTO cells.

Capacity Retention of LFP/Graphite Cells Cycled at 30°C

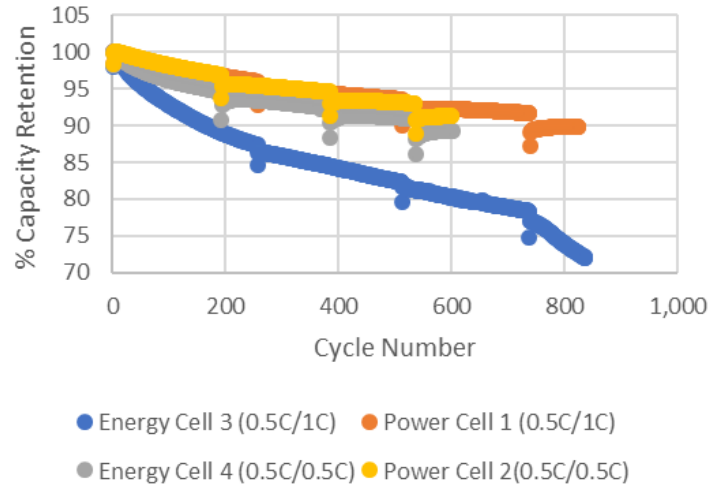


Figure 11. LFP/graphite cycling results.

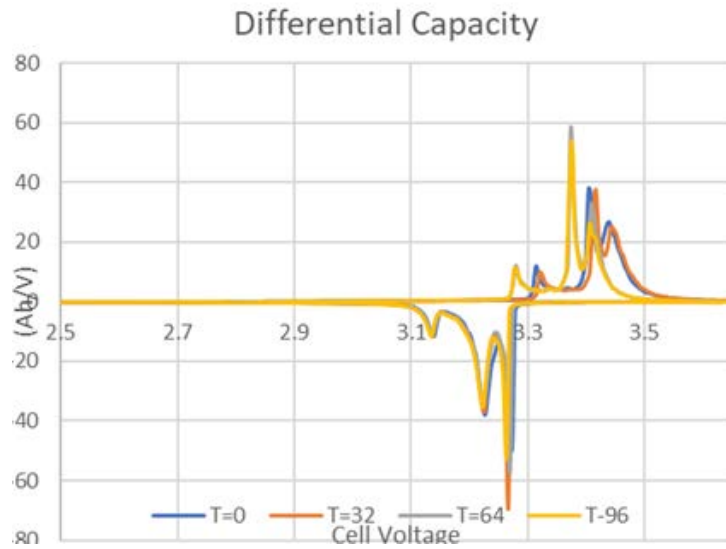


Figure 12. Differential capacity test for LFP/graphite cells.

HPPC results show that as the cell continues to cycle, it loses its ability to deliver power at low SOCs. Understanding this phenomenon will be critical for predicting end-of-life behavior of these cells. The differential-capacity results suggest that the loss of performance is most likely attributed to changes in the graphite anode. This is a known problem. Graphite is known to degrade from extensive cycling. In an effort to predict the lifetime of these cells, a simple trend line (which is an overestimate) was fitted to each curve in Figure 11 and the calculated slopes of the line can be found in Figure 13. These fade rates fall short of providing 10,000 cycles, even when allowing for 50% capacity loss at end of life.

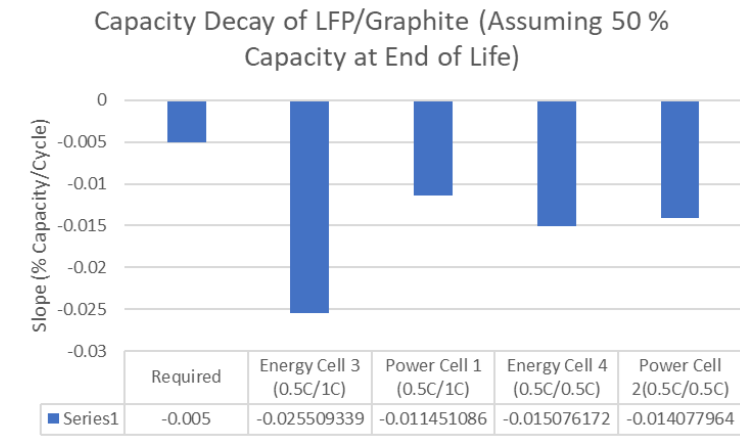


Figure 13. Capacity decay rate for each LFP/graphite cell type and condition.

Summary

Cycling under the initial protocol has shown that the commercial NMC/graphite and LFP/graphite cells, designed for purposes other than the proposed BTMS system, are not capable of meeting a 10,000 cycle life goal. Design tradeoffs taken to enhance properties (e.g., energy density) that are not critical to the BTMS application may impact their performance relative to BTMS goals. As material and design factors are investigated to address cost and cycle life, which are primary BTMS technology gaps, we will continue to develop updated testing methods to provide accelerated results that are relevant to target operating scenarios developed through modeling. The testing effort will be closely coupled with complementary machine-learning development tasks aimed at minimizing the time-on-test needed to accurately predict lifetime.

Physics-Based Machine Learning for Behind-the-Meter Storage

Idaho National Laboratory and National Renewable Energy Laboratory

Eric Dufek, Kandler Smith, Ross Kunz

Background

Developing and deploying batteries in new, diverse applications requires that the batteries function in the necessary environment as well as a deep understanding of their performance, life, and expected failure mechanisms. In the past, the primary means to advance knowledge on performance and life was to test batteries for extended periods of time under a range of different scenarios. Testing of batteries in this manner can take upwards of a year to make reasonable estimations of life and to clearly identify failure modes and rates. The need to shorten the design and testing cycle is critical to bringing new battery chemistries and cell designs into emerging applications such as stationary energy storage to support EV charging stations capable of extreme fast charging. Connection of physics-based life models and machine learning (ML) provides the opportunity to enable more robust assessment of battery aging, identification of failure mechanisms, and understanding as new use-case scenarios are proposed. The current project focuses on ways to apply ML to enhance the estimation of life while also identifying key failure pathways. During the first portion of the project, existing datasets will be used for both training and validating ML approaches to better characterize expected battery life. The work also looks to link ML with existing physics-based life models at INL and NREL.

Results

During Q4, three primary activities were advanced toward adapting physics-based lifetime models to use ML tools to automate the process of more rapidly and accurately mapping accelerated test results to real-world lifetime predictions: 1) data transfer and analysis, 2) life model generalization, and 3) machine learning using existing datasets. Across each of these three areas, INL and NREL teams have had significant interaction to drive uniformity in analysis and to advance the overall knowledge base in the project.

Data exchange. For test datasets, the team exchanged data from 2012 Nissan Leaf cell and pack fast-charge experiments (INL) [1], as well from Kokam 75-Ah graphite/NMC grid energy storage cell life testing (NREL) [2]. These cycling sets each provide distinct information from prior testing efforts at different cycling conditions and temperature. Combined, they were chosen for these reasons as well as for their combination of summary (associated with reference performance tests) and raw data from the different cycling regimes. Initial sharing of datasets has occurred using Box, with plans in place to move forward with different sharing mechanisms during FY20.

Generalize physical lifetime model. NREL generalized and documented their battery lifetime predictive model based on experience from previous Li-ion technologies [2,3]. With some exceptions, changes in battery performance metric, y , are represented as a linear combination of the reduced-order degradation models x_i shown in Table 1,

$$y = \sum_i x_i.$$

Performance metrics y include battery relative resistance growth r ; relative capacity q ; or, in the case of changing mechanisms controlling capacity fade, y may represent negative electrode site inventory q_- , positive electrode sites inventory q_+ , and lithium inventory q_{Li} with overall relative capacity taken as

$$q = \min(q_{Li}, q_-, q_+).$$

In Table 1, x is the state variable for degradation mechanism i , p is the order of the fade mechanism (a constant), k is the rate of fade, and M is the magnitude of fade. Accelerated aging tests are generally conducted at different constant values of temperature T , depth of discharge DOD , average state of charge SOC , and discharge/charge current C_{rate} . For individual aging tests under simple aging, fade rate k is constant, and the analytical solution is used for model fitting. With fade rate k determined for multiple aging conditions, a rate-law model is fit to describe $k(T, SOC, DOD, C_{rate})$. Rate laws are generally built as multiplicative combinations of acceleration factors listed in Table 2,

$$k_i = k_{i,ref} \prod_j \theta_j.$$

Table 1. Degradation mechanism models

Mechanism	State equation	Analytical solution valid for constant k
1) Mixed diffusion/kinetic-limited side reaction ¹	$\dot{x}(t) = kp \left(\frac{k}{x(t)} \right)^{\left(\frac{1-p}{p} \right)}$	$x(t) = kt^p$
2) Site loss ²	$\dot{x}(N) = k' \left(\frac{x_0}{x(N)} \right)^p$	$x(N) = [x_0^{1+p} + k' x_0^p (1+p)N]^{\frac{1}{1+p}}$
3) Break-in process ³	$\dot{x}(t) = k(M - x(t))$	$x(t) = M(1 - \exp(-kt))$

1. Order $p = 0.5$ for diffusion-limited solid/electrolyte interface (SEI) growth.
2. Order $p = 0$ for linear fade. $p \geq 1$ for accelerating fade.

Table 2. Acceleration factors used for building degradation rate laws

Rate/magnitude dependence	Type of Stress	Acceleration factor, θ_j
Temperature	Chemical & Mechanical	(1.1) $\exp \left[-\frac{E_a}{R_{ug}} \left(\frac{1}{T(t)} - \frac{1}{T_{ref}} \right) \right]$
SOC	Chemical	(2.1) $\exp \left[\frac{\alpha F}{R_{ug} T(t)} \eta(t) \right]$ where $\eta(t) = U_{\pm}(t) - U_{ref}$
C-rate	Chemical	(2.2) ... where $\eta(t) = U_{\pm}(t) - U_{ref} - C_{rate}(t)R_{film}$
	Mechanical	(3.1) $C_{rate,i} \sqrt{t_{pulse,i}} = DOD_i \sqrt{C_{rate,i}}$ (3.2) $(C_{rate,i})^y$
DOD	Chemical	(4.1) $(DOD_i)^\beta$
	Mechanical	(5.1) $(1 + \gamma(DOD_i)^\beta)$ (5.2) $\exp(\gamma(DOD_i)^\beta)$

- a. i is cycle index from Rainflow algorithm

- b. Fitting parameters are k_{ref} , E_a , α , R_{film} , γ , β
- c. Constants are $R_{ug} = 8.314 \text{ J K}^{-1} \text{ mol}^{-1}$, $F = 96485 \text{ C mol}^{-1}$, T_{ref} arbitrary with units [K], U_{ref} arbitrary with units [V]
- d. U_- and U_+ , respectively, are negative and positive electrode equilibrium potentials, and are functions of SOC.

The generalizations described above were used to refine life model parameters for graphite/NMC cells. The first step of this activity took place under the DOE’s eXtreme Fast Charge and Cell Evaluation of Lithium-Ion Batteries (XCEL) program using the Kokam 75-Ah cell data. This was then transferred to the Nissan Leaf cell data from INL (Figure 1) across three temperatures and three charge protocols. INL and NREL are both using the initial life model analysis as the base set for work related to ML using physics-based analysis and development.

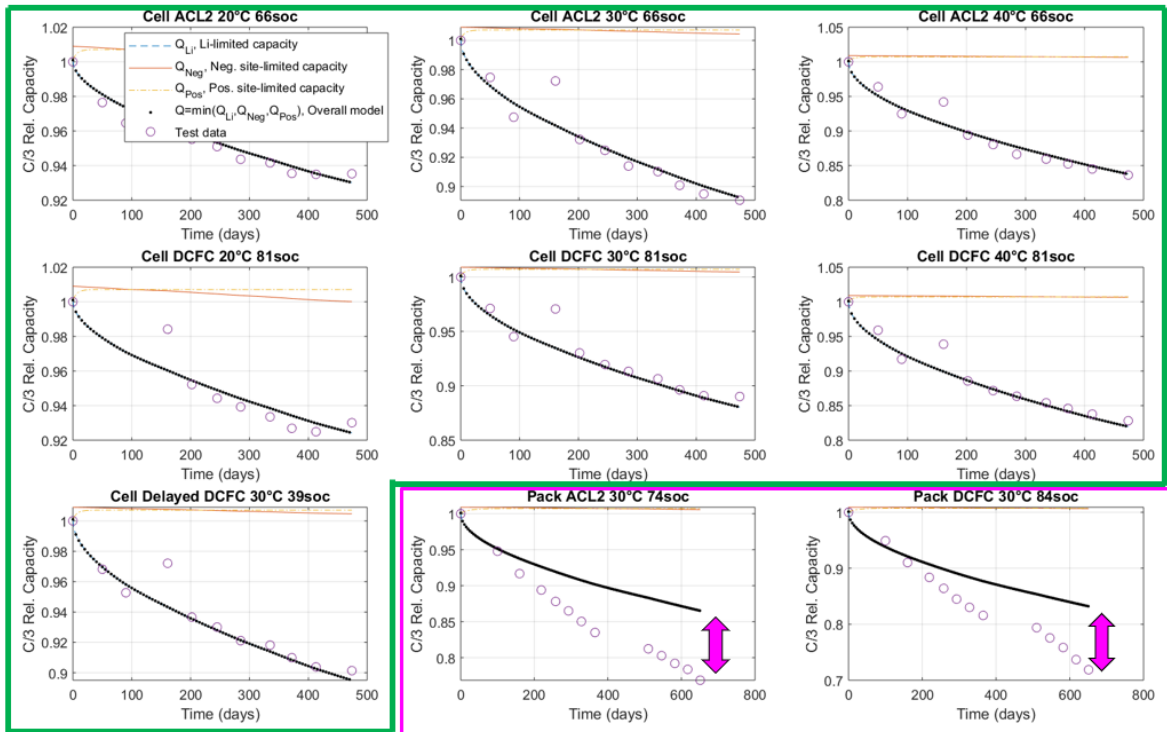


Figure 1. Example of physics-based life predictive model (NREL) applied to 2012 Nissan Leaf fast charge data (INL).

Machine learning of physics-based life model from summary capacity/resistance data. With numerous possible degradation mechanisms (Table 1) and dependence on operating conditions (Table 2), identifying a life model from accelerated aging data is a time-consuming process. As a first step to automate the life model identification, the team applied the elastic net regularization algorithm to one step of the model-fitting process for the Kokam data. Popular in the ML field for its robustness in model selection, the elastic net algorithm efficiently eliminates or “turns off” extraneous terms in a model with little statistical significance. Figure 2 shows possible fitted-model coefficients versus the regularization parameter, lambda. Many possible coefficients can reasonably represent the data, but some are unrealistic (e.g., producing negative fade rates such as the “best fit” minimum mean-square error model coefficients in green in Figure 2). Instead, the elastic net selects more reasonable parameters within 1 standard error of the data and eliminates unneeded terms in the model. In the next quarter, the team will apply the algorithm to additional steps of the model-fitting process to automate robust life model identification.

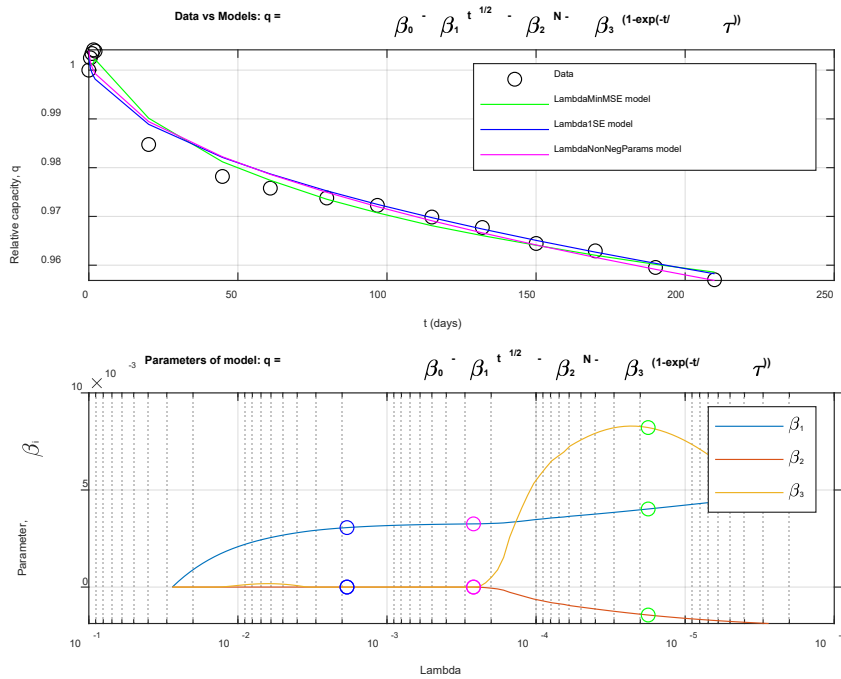


Figure 2. Example local model fit of Kokam 75-Ah cell data using machine-learning elastic-net regularization algorithm.

Machine learning of physics-based life model from raw electrochemical current/voltage data. The second ML-based activity focused on analysis using the raw electrochemical data from the Nissan Leaf dataset. Of the data used for analysis, key portions were used of the cycling profiles and rest steps. Broadly, the key points of interest were chosen due to alignment with key kinetic and thermodynamic indicators including cell impedance, state of charge, and temperature.

During early stages of the ML work, a key need identified when considering and linking physics with the life model was the need for a robust analysis that clearly assessed the adequacy of the sample set and also differentiated outliers. Figure 3 presents an example of a voltage measurement used for ML before (orange) and after removal of outliers (blue).

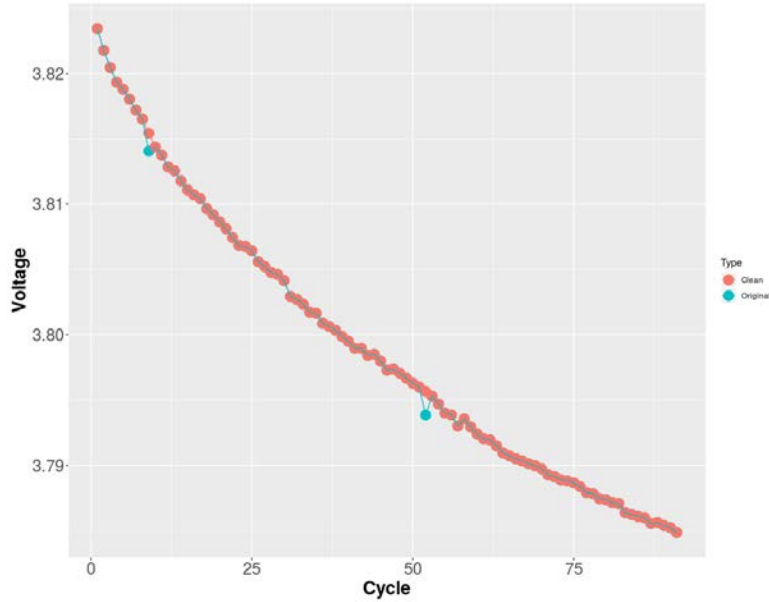


Figure 3. Voltage measurement as a function of cycle using the original data (blue) and clean data after removal of data outliers (orange).

For the initial set of analyses, the use of different ML algorithms proceeded using the cleaned dataset. Figure 4 shows the $C/20$ capacity from the reference performance test at the end of 900 cycles for the training and predicted data. Figure 4 shows good agreement between the training and predicted sets. Further confirmation of the utility of the ML algorithms was achieved by comparing the predicted value for each of the different cycle conditions with the actual experimentally measured capacity during the reference performance test at 900 cycles (Figure 5).

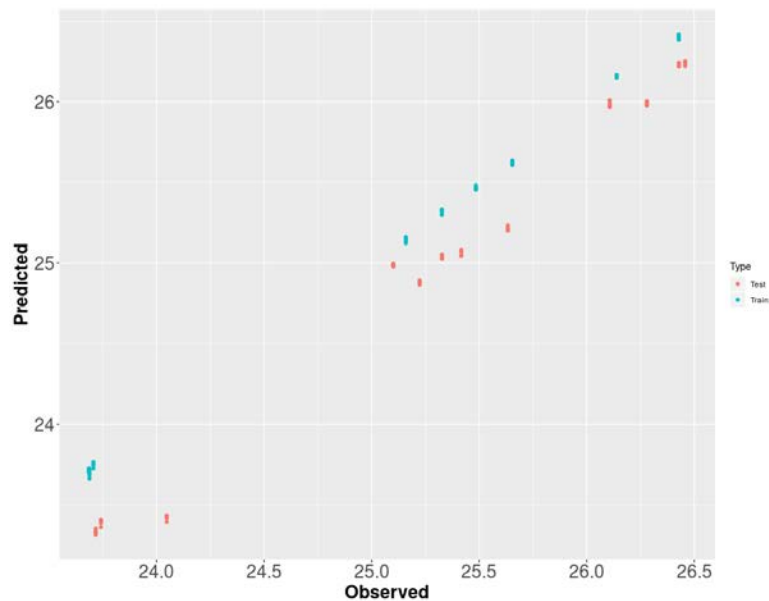


Figure 4. Comparison of predicted and observed reference performance test capacity after 900 cycles for the test and training datasets. Analysis performed using Nissan Leaf test data.

Figure 5 shows good alignment between the different cycling conditions due to the physically linked parameters used for the ML. Distinct about the analysis is that the cycle sets included data from three different cycling temperatures and three different charge procedures (AC Level 2, DC Fast Charge, and a combination of the two) [1]. Continued work in this area focuses on refining the analyses and further linking the life model as described above.

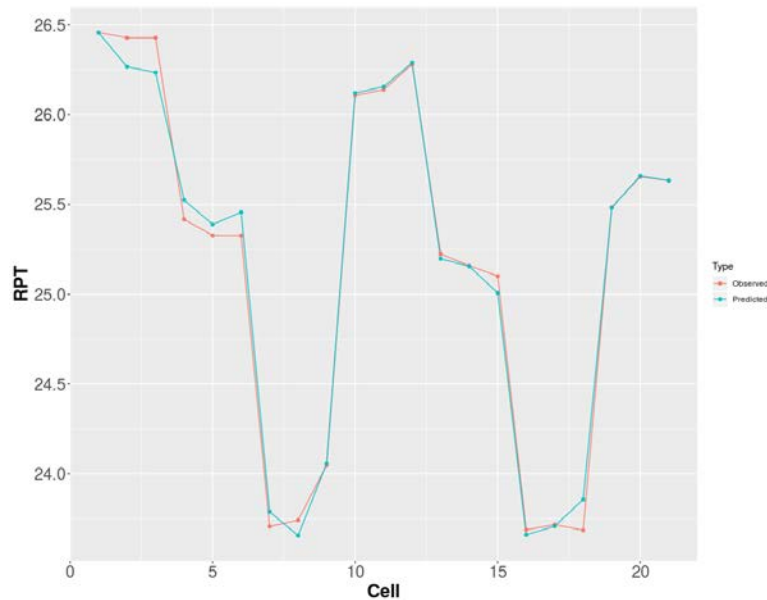


Figure 5. Comparison of observed and predicted reference performance test capacity for each cell in the analysis. Of note is that the data were collected at three different temperatures and three different cycling conditions [1].

Conclusions

The team achieved significant progress in physics-based ML of life-predictive models during Q4 of FY19. During the second quarter of the project, two datasets were effectively shared between INL and NREL. One dataset was used to refine life model parameter estimation to reduce the time needed to execute and adapt the model for different cell designs and chemistries. The other dataset was used to predict capacity fade as a function of aging using small quantities of cycling data that are linked to specific kinetic and thermodynamic aging processes in the batteries. Current work is linking together the two methods.

References

- [1] T.R. Tanim, M. Shirk, R.L. Bewley, E.J. Dufek, B. Liaw, “Fast Charge Implications: Pack and Cell Comparison and Analysis,” *J. Power Sources*, 381 (2018), 56–65.
- [2] K. Smith, A. Saxon, M. Keyser, B. Lundstrom, Z. Cao, A. Roc, “Life Prediction Model for Grid-Connected Li-Ion Battery Energy Storage System,” *American Control Conference*, Seattle, WA, May 30–June 1, 2017.
- [3] S. Santhanagopalan, K. Smith, J. Neubauer, G.-H. Kim, A. Pesaran, M. Keyser, *Design and Analysis of Large Lithium-Ion Battery Systems*, Artech House, Boston, 2015, ISBN-13: 978-1608077137.

APPENDIX

I Behind-the-Meter Energy Storage for Buildings

I.1 Introduction

Behind-the-meter storage (BTMS) is needed at buildings to mitigate high electric demand charges and to facilitate building-sited renewables and electric vehicle (EV) charging. BTMS systems can include electrochemical and/or thermal, but determining which to use—and how to size and control them together—is largely unknown.

To determine system designs for thermal and battery energy storage systems, we will use a framework that includes *multi-scale modeling* and *multi-scale experiments* for designing, sizing, characterizing, and evaluating BTMS systems, including thermal storage at multiple scales. The multi-scale experiments to validate the models are critical and ensure that the thermal + battery storage system results are meaningful and accurate. This project's goal is to evaluate today's available thermal + battery storage solutions, future possible system-level solutions, and the thermal storage R&D needs to enable these future solutions.

This section summarizes research performed in FY19 on the above topics. Specifically, it covers:

1. Thermal storage material characterization
2. Thermal storage device characterization
3. Integration and controls of thermal and battery energy storage

I.2 Thermal storage material characterization

Traditional thermal energy storage shifts electricity use from day to night using large, custom systems, which have high initial costs for planning, engineering, and installation. Thermal energy storage that is instead integrated into a packaged system eliminates the initial cost for custom design and installation.

Solid/liquid phase-change materials (PCMs) can be designed for these packaged applications, but have several limitations, including low thermal conductivity and the need for a tank or other type of leak-free containment. PCMs with a solid-to-solid transition (e.g., amorphous to crystalline phase transformation) can overcome these limitations, but their energy densities are low, typically less than 100 J/g. An alternative is a solid/liquid PCM that is made into a solid-state composite PCM (Figure 1). This composite PCM maintains its solid shape upon melting (the PCM remains in the nanoscale pores), provides nearly a 100x increase in thermal conductivity, and has an effective latent heat of 150-200 J/g. These composite PCMs are created by expanding natural graphite through rapid heating, after intercalation with an acid. The expanded graphite is then compressed, creating these porous graphite structures that are then soaked in PCM to create the composite PCM.

The thermal-conductivity enhancement of these composite PCMs exceeds the commonly used approach of adding thermally conductive fillers (~2-3x), which lack an interconnected (or percolated) thermal network. These composite PCMs can be well-suited for the packaged systems mentioned above, but more data are needed to evaluate their performance. The key material properties we measured were:

- Thermal conductivity
- Heat of fusion and transition temperature
- Thermal cycling performance

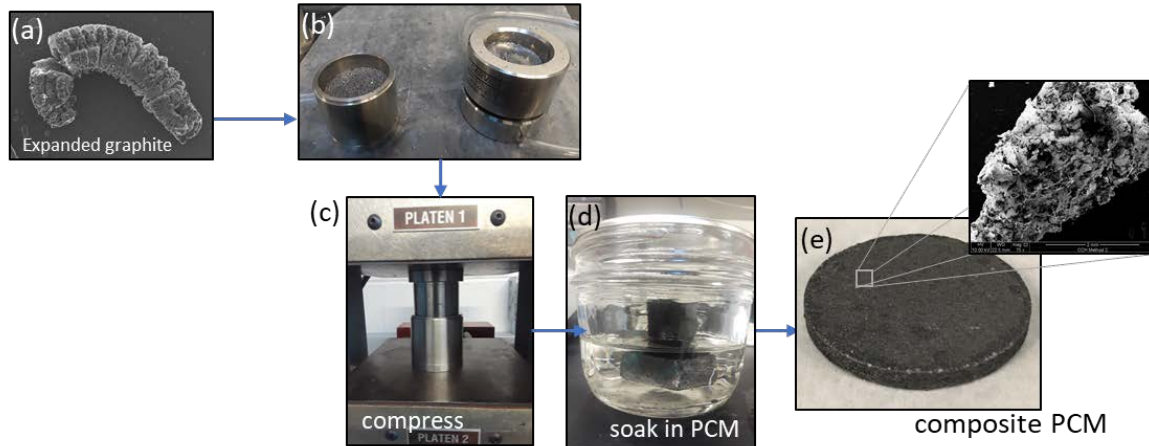


Figure 1. (a) Expanded graphite (EG), thermally expanded after acid intercalation. EG flakes are compressed in (b) die fixture using (c) pneumatic press. (d) Graphite matrix is soaked in PCM, resulting in (e) composite PCM.

Thermal conductivity. In addition to energy density, thermal conductivity (k) is an important figure of merit for thermal storage applications. Higher thermal conductivity enables faster charge/discharge rates, resulting in higher power densities. Tetradecane is an organic paraffin PCM that suffers from low k (~ 0.1 – 0.4 W/m-K). Incorporating it into the nanoporous graphite structure greatly improves k .

The k of graphite matrices with and without infiltrated PCM were measured using a combination of measurement approaches. The ASTM D-5470 steady-state method was used to measure the k of 80% porous graphite. It was found that there is anisotropy in the k of the samples, with k being higher in the direction perpendicular to compression than the direction parallel to compression. For a sample with no PCM, k was measured to be 8.9 W/m-K in the parallel direction and 17.4 in the perpendicular direction. A sample with PCM infiltrated was measured to be 9.7 W/m-K in the parallel direction. This indicates that because the pure PCM k is so low, the composite k is dominated by the graphite and the k of the samples with and without PCM are similar. A different sample of graphite matrix with no PCM, of about 92% porosity, was measured using the transient plane source (TPS) technique. This sample was measured to have k 11.7 W/m-K in the parallel direction. Inserting the PCM into the graphite matrix increases thermal conductivity by 50x.

Heat of fusion and transition temperature. The specific PCM studied here is n-tetradecane ($C_{14}H_{30}$), an organic paraffin PCM with transition temperature of 4°C which is suitable for air-conditioning applications. Figure 2 shows several differential scanning calorimeter (DSC) curves of PCM composites with varying mass fraction of PCM and graphite, and Table 1 presents their corresponding heats of fusion and transition temperatures. As can be seen, incorporation of graphite does reduce latent heat of fusion (energy density) of the PCM composite, relative to the pure PCM. However, as discussed in the previous section, incorporation of just 20% graphite results in up to 50x increase in thermal conductivity, but only $\sim 20\%$ reduction in heat of fusion.

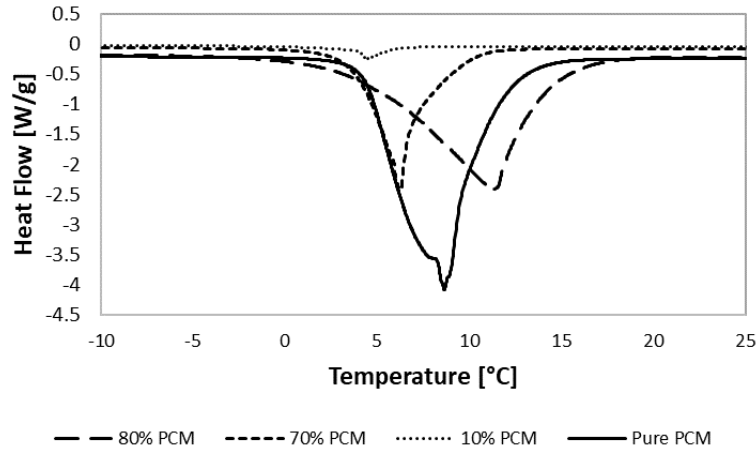


Figure 2. DSC curves (melting) of several PCM composites with varying mass fraction of PCM

The incorporation of graphite does not change the transition temperature of the PCM, as shown in Table 1, indicating no chemical interaction between the graphite and the PCM.

Table 1. Heat of fusion and transition temperature of several PCM composites with varying mass fraction of PCM

Sample	T_i [°C]	ΔH_f [J/g]
Pure PCM	4.16	213.4
80% PCM/20% graphite	4.02	183.0
70% PCM/30% graphite	4.61	97.8
10% PCM/90% graphite	3.94	6.2

Dynamic performance and cycling behavior. In addition to the material properties above, we also designed, fabricated, and commissioned an experiment enabling measurements of heat transfer through the graphite-tetradecane composite PCM. This allows us to estimate thermal conductivity, heat of phase change, and the transition temperature of bulk TES materials, unlike the techniques above, which are constrained to small sample sizes. The experiment can also characterize the thermal cycling behavior of the composite PCM. A numerical heat-transfer model developed for comparison showed good agreement with experimental data.

The experiment consists of a heat source and sink as two fluid-filled plates connected to temperature-controlled baths (Figure 3, left). The sample to be characterized is placed between the plates with silicone elastomer pads as a thermal interface material (Figure 4, right). Insulation along the sides ensures one dimensional heat transfer through the sample.

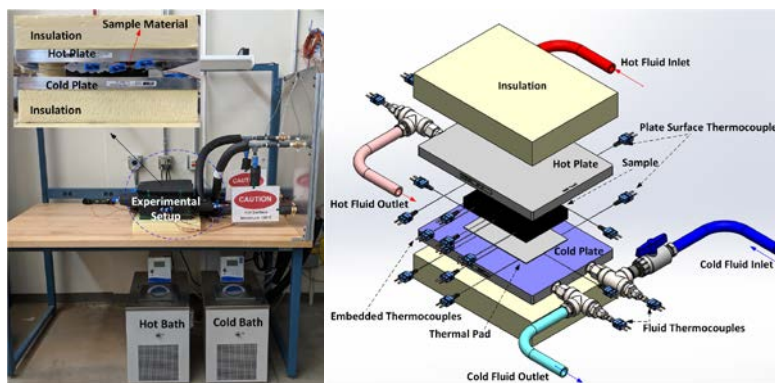


Figure 3. Experimental setup (left), and CAD rendering showing each component

The flow rate of the heat-transfer fluid was controlled using a manual gate valve. Temperature and flow rate measurements were used to calculate heat-transfer rates. Surface thermocouples were placed on both top and bottom surfaces between the composite PCM sample and the heat-transfer plates and were used to estimate thermal conductivity. Embedded thermocouples along the centerline of the composite PCM sample allowed measurement of the temperature of the material and helped identify the transition temperature and the completion of the charging/discharging process.

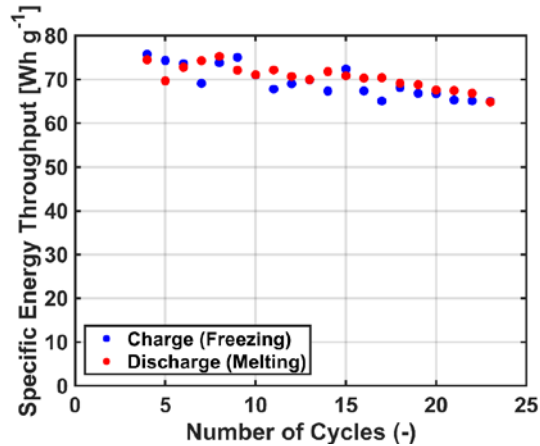


Figure 4. Energy storage capacity during cycling.

Initial results from thermal cycling experiments (Figure 4) showed a degradation in specific energy storage capacity by ~15% after 23 cycles. We observed leakage of the PCM from the composite material during multiple cycles, causing the degradation in the storage capacity. During these experiments, we observed consistent phase-transition temperature for this material at ~4.5°–5°C, which agreed well with other measurements using DSC.

We are currently modifying the experiment to ensure isothermal conditions of the heat source and sink surfaces, automating the flow control valves for improved cycling control, and developing methods to minimize thermal contact resistance by applying a consistent clamping force and identifying the most suitable thermal interface material.

Conclusions and potential next steps. The investigated composite PCMs show promise for thermal energy storage applications. From the above results, we conclude that:

- Composite PCMs show a large increase in thermal conductivity even for high-porosity graphite structures (>80% open volume).
- The method of creating these graphite composite PCMs leads to anisotropic thermal conductivity, with ~2x difference between the compression and non-compression directions.
- Although these materials maintain their shape, slow leakage needs to be prevented through sealing or packaging techniques.
- Contact resistance between the PCM composite and the heat-transfer surfaces are critical for the overall performance of these thermal storage devices.

Based on this research, we recommend the following next steps:

1. **Improved graphite host matrices.** More research is needed to better understand and improve the graphite host matrices, including infiltrating PCM and obtaining higher thermal conductivity with maximal porosity. This requires experiments and modeling. The experiments will characterize the structure of existing and new graphite host matrices, including pore size, pore size distribution, tortuosity, total open volume, accessible volume, and pore interconnectedness. These properties are difficult to measure with existing techniques, including intrusion porosimetry or BET. Micro-scale modeling will help identify the impact of changes to the graphite structure, and ideally determine the preferred structure through multiple model simulations.
2. **Reducing contact resistance.** The importance of contact resistance is evident through multiple projects working with this composite PCM. An inexpensive solution is needed to address this issue if

this technology is to be commercialized. We are investigating thermal interface materials, composite PCM geometries, and applying pressure to reduce this contact resistance—both for implementing this PCM in practice and for minimizing error in our thermal measurements.

3. **Cycling behavior.** The cycling performance of these composite PCMs is still unknown. Initial experiments showed some degradation, but some (if not all) of this was due to leakage of the PCM. Further experiments need to eliminate this leakage to enable measurement of long-term cycling degradation. In addition, we need to develop experiment protocols to ensure we capture all the relevant degradation mechanisms.
4. **Selectable transition temperature.** The PCM investigated here has a phase-transition temperature of 4°C , which is suitable (although not optimal) for air-conditioning applications. There are many organic and inorganic PCM options, spanning the -30°C to 80°C range applicable to buildings. But their performance, particularly when impregnated within the graphite matrices, needs more research.

I.3 Thermal storage device characterization

As with electrochemical batteries, one needs to understand not only the *material* properties of thermal storage, but also the performance when integrated into a *device*. The charging and discharging of thermal energy storage devices is analogous to the charging and discharging of electrochemical devices. The analogy is best illustrated with example discharge curves for electrical storage using electrochemical batteries and a capacitor, and for thermal storage using a sensible material and phase-change material (Figure 5). The discharge curves for sensible storage (left) and an electric capacitor (right) have similar behavior, with their characteristic exponential decay in potential. Phase-change materials behave more like electrochemical batteries, with their slower decay in potential, because of the energy released or absorbed by the enthalpy of fusion during phase change.

For thermal storage, the temperature drop in potential is from “ qR ” losses, similar to iR losses for electrochemical batteries. The decay in temperature potential is caused by two effects: 1) at high and low state-of-charge, the PCM behaves more like a capacitor, with sensible storage above or below the phase-transition temperature, and 2) the finite temperature gradients that occur within the storage material mean that the melt (or freeze) front is further from the heat-transfer fluid, increasing the resistance between the fluid and the phase-change process. Like batteries, the potential can recover if the discharge is interrupted by equalizing temperature gradients within the material.

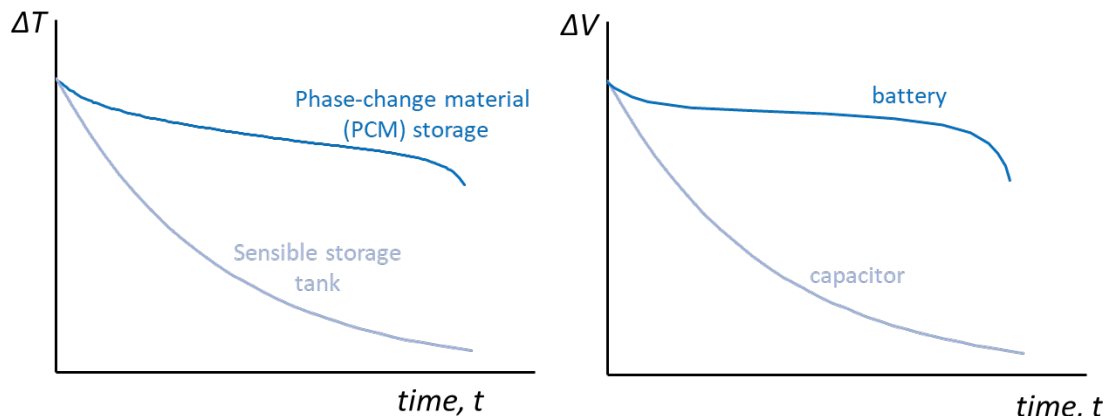


Figure 5. Illustrative discharge curves for sensible and latent thermal storage materials (left) and for electrochemical and capacitor energy storage (right). This shows a drop in potential during discharge, with sensible storage and capacitors losing their potential more quickly than phase-change and electrochemical storage.

Furthering this analogy, we can create Ragone plots for thermal energy storage using discharge curves at different C rates. Figure 6 shows illustrative discharge curves for electrochemical energy storage (top, left),

and the corresponding Ragone plot (top, right). Constant-power discharge curves for phase-change thermal energy storage (bottom, left) are also used to create corresponding Ragone plots for thermal energy storage (bottom, right). The Ragone plots require an assumed *cutoff temperature*, similar to the *cutoff voltage* used for electrical storage.

In FY20, we will further explore these thermal discharge curves and Ragone plots to better understand the mechanisms that cause the drop in temperature potential at high depth of discharge and at high C rates. We will also develop design rules for thermal storage devices for different C rates.

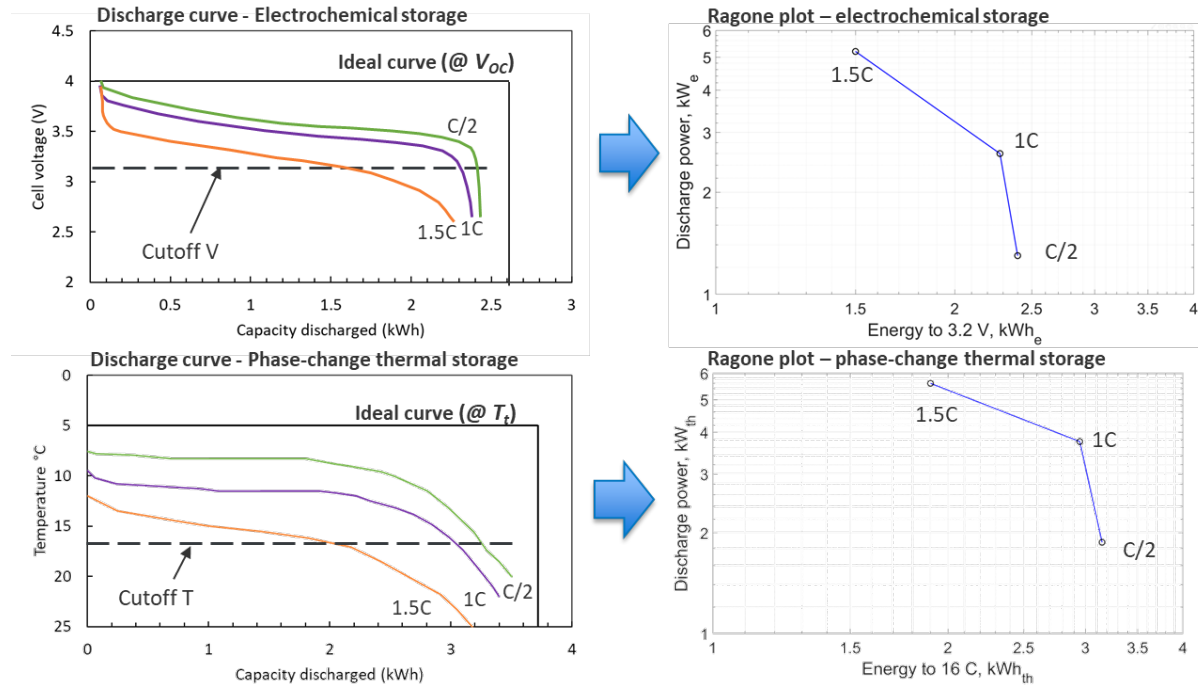


Figure 6. Discharge curves at different C rates, and corresponding Ragone plots for electrochemical batteries (top) and phase-change thermal energy storage (bottom). V_{oc} = open-circuit voltage; T_t = transition temperature. The y-axis on the bottom-left plot is inverted because these data are for cooling applications.

I.4 Thermal storage device characterization

In FY19, we designed and started construction on a new capability in NREL’s Energy Systems Integration Facility (ESIF) to characterize thermal storage technologies. Specifically, this capability enables characterization at the device and system scales:

1. Thermal characterization experiments enable us to characterize the performance of components and systems, over a range of operating conditions (e.g., flow rates, temperatures, humidity (if applicable)). For example, we can generate curves of charge rates, discharge rates, and efficiency vs. temperature.
2. Hardware-in-the-loop (HIL) experiments enable us to measure the performance of components and systems while representing surrounding components in simulation. An example is given below, where we can emulate a building’s thermal and electric loads for a specific climate, but include the chiller plant and thermal storage tank in hardware. This gives us insight into the actual performance of the system when installed in a representative environment, but without the need for a field demonstration, and with certain equipment in simulation. For example, in Figure 7, the solar photovoltaic system is shown in simulation, while the battery is in hardware. But these could be switched, depending on which question is being answered.

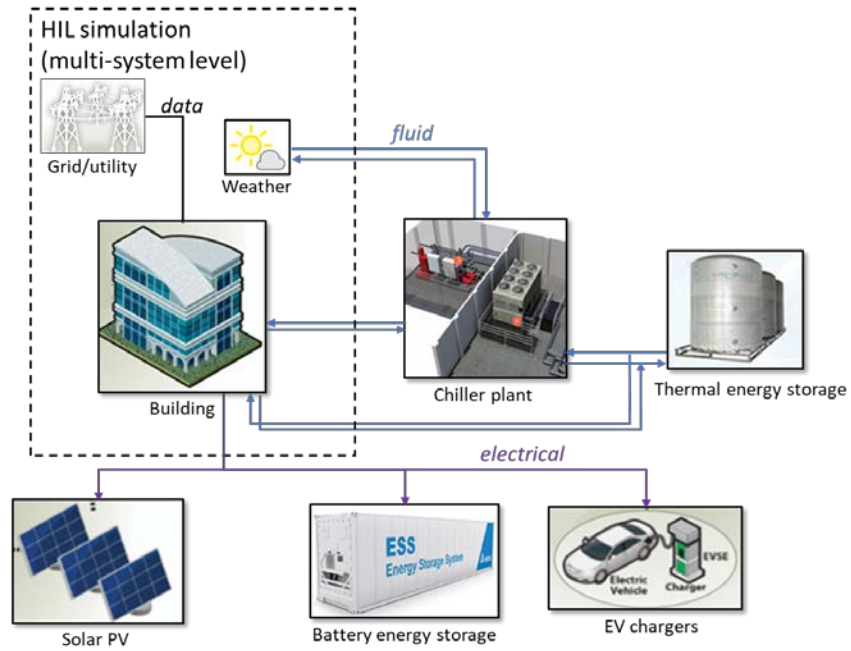


Figure 7. Experimental hardware in the loop (HIL), focusing on multi-system level integration of the building and behind-the-meter storage assets. In this case, storage assets are in hardware, with the building, grid, and photovoltaics (PV) simulated. The conditions applied to the hardware is from these simulations or from a specified weather file.